International Journal of Heat and Mass Transfer 106 (2017) 103–126

Contents lists available at ScienceDirect

International Journal of Heat and Mass Transfer

journal homepage: www.elsevier.com/locate/ijhmt

Review

Review of drop impact on heated walls

Gangtao Liang [a,b], Issam Mudawar [b,*]

[a] Key Laboratory of Ocean Energy Utilization and Energy Conservation of Ministry of Education, School of Energy and Power Engineering, Dalian University of Technology, Dalian 116024, China
[b] Purdue University Boiling and Two-Phase Flow Laboratory (PU-BTPFL), School of Mechanical Engineering, 585 Purdue Mall, West Lafayette, IN 47907, USA

ARTICLE INFO

Article history:
Received 19 August 2016
Received in revised form 6 October 2016
Accepted 8 October 2016
Available online 21 October 2016

Keywords:
Drop impact
Drop evaporation
Drop rebound
Secondary droplets
Leidenfrost point

ABSTRACT

This paper provides a comprehensive review of published literatures concerning the fluid mechanics and heat transfer mechanisms of liquid drop impact on a heated wall. The review is divided into four parts, each centered on one of the main heat transfer regimes: film evaporation, nucleate boiling, transition boiling, and film boiling. Each of these regimes is discussed in detail in terms of available depictions of drop deformation and/or breakup, proposed heat transfer mechanisms, predictive correlations and/or models. It is shown that understanding the underlying physics for each heat transfer regime is highly dependent on the experimental methods that investigators have adopted, and broadness of available databases in terms of liquid type, drop size and momentum, impact angle, and wall material and surface roughness. Despite significant advances in experimental, theoretical and computational research in understanding the interfacial behavior of the drop from the moment of impact, there are many inconsistencies concerning some of the most important aspects of the impact process and ensuing heat transfer, especially in regards to critical heat flux, transition boiling, and the Leidenfrost point. This review is concluded with recommendations concerning future work that is needed to address poorly understood and/or contradictory issues.

Contents

* Corresponding author.
E-mail address: mudawar@ecn.purdue.edu (I. Mudawar).
URL: https://engineering.purdue.edu/BTPFL (I. Mudawar).

http://dx.doi.org/10.1016/j.ijheatmasstransfer.2016.10.031
0017-9310/

Nomenclature

Bo	bond number
C	coefficient
c_p	specific heat at constant pressure
D	spreading diameter
d	diameter
D^*	non-dimensional spreading diameter
d_{32}	Sauter Mean Diameter
g	gravitational acceleration
h	heat transfer coefficient
h_c	convective heat transfer coefficient
h_{fg}	latent heat of vaporization
h^*_{fg}	modified latent heat of vaporization
Ja	Jacob number
k	thermal conductivity
m	defect size
N	number of secondary droplets
n	exponent
Nu	Nusselt number
Oh	Ohnesorge number
P	pressure
Pr	Prandtl number
Q	heat transfer rate
q''	heat flux
R	radius of wetted area
r	radial coordinate
Re	Reynolds number
R_a	average surface roughness
R_z	height of surface roughness feature
T	temperature
t	time
V	drop volume
v	velocity
v^*	dimensionless velocity
v_{sound}	speed of sound in liquid
We	Weber number
x	vapor molar fraction
z	axial coordinate

Greek symbols

α	thermal diffusivity; average ejection angle of secondary droplets
β	coefficient
δ	vapor layer thickness
δ^*	dimensionless vapor layer thickness
ε	mass diffusivity
μ	viscosity
ϕ	impact angle
ρ	density
σ	surface tension
τ	non-dimensional time
θ	contact angle
θ_r	receding contact angle
θ_0	initial contact angle

Subscripts

b	drop base
c	critical
contact	liquid–solid contact
drop	liquid drop
e	evaporation
f	liquid
g	gas
i	interface; inclined
L	Leidenfrost
L, d	dynamic Leidenfrost
L, i	dynamic Leidenfrost for inclined impact
max	maximum
n	normal
min	minimum
o	oscillation
r	residence
sat	saturation
v	vapor
w	wall

1. Introduction

1.1. Background

The phenomenon of drop impingement is found in numerous industrial applications, besides being a common occurrence in nature. The importance of this phenomenon has spurred numerous investigations by researchers over many decades in pursuit of detailed understanding of mass, momentum, and heat transfer interactions. But despite these efforts, there is continued interest in all aspects of this topic among researchers, who are taking advantage of modern advances in ultra high-speed imaging coupled with fluid flow and heat transfer diagnostics tools [1–3]. In general, the topic of drop impact can be classified into three main subtopics based on impingement target: solid wall, liquid film (pre-wet wall), and deep liquid pool. Progress in these subtopics can be found in review articles by Prosperetti and Oguz [4], Rein [5], Yarin [6], Marengo et al. [7], Moreira et al. [8], and Josserand and Thoroddsen [9]. The present review is focused on drop impingement on a solid heated wall.

Most applications of drop impingement involve relatively high temperatures, while a few concern maintaining relative low wall temperatures. Examples include fuel drop impingement in internal-combustion engines with direct fuel injection [10], saline drop impact on heat transfer tubes of falling-film evaporators in desalination and refrigeration [11], water droplet impingement on steam turbine blades and in quenching metal castings and extrusions [12], and spray cooling in fire extinguishing and electronics cooling systems [13]. However, the focus of published drop impingement review articles has been mostly on adiabatic impact dynamics, rather than on heat transfer and phase change processes. Therefore, this article will focus on drop impingement on heated walls.

1.2. Complexity of drop impingement on heated walls

In 1966, Wachters and Westerling [14] conducted pioneering experiments involving drop impact on a heated wall within the film boiling regime. Since then, great strides have been made, aided by new advances in both instrumentation and computational tools. Overall, numerous parameters can influence this process, including drop parameters (diameter, d_{drop}, impact velocity, v_{drop}, and physical properties of liquid, such as saturation temperature, T_{sat}, density, ρ_f, viscosity, μ_f, and surface tension, σ), surrounding gas parameters (pressure, temperature, properties, velocity, and flow configuration), and wall characteristics (wettability, diffusivity, surface roughness, and wall temperature, T_w).

Heat transfer in drop impingement on a heated wall is strongly influenced by magnitude of wall temperature relative to the liquid's saturation temperature. When T_w is below T_{sat}, heat transfer is dominated by heat conduction from the wall to the liquid, and evaporation due to mass transfer along the liquid–gas interface. And uneven drop temperature can result in internal flow caused by the Marangoni effect [15,16]. Additionally, drop-wall contact area, contact angle, and heat flux vary greatly during the impact.

When T_w begins to exceed T_{sat}, the drop boils on the heated wall, and small bubbles form inside the drop, which grow and merge, but do not uplift from the wall. This bubble behavior is distinctly different from that encountered in pool boiling, where bubbles are quickly removed from the wall by buoyancy. Moreover, bubble size, evolution, distribution, and merger greatly influence flow dynamics and drop heat transfer. At even higher wall temperatures, when T_w exceeds the Leidenfrost temperature, T_L, a thin micrometer-scale vapor layer quickly forms between the drop and the wall, which greatly decreases liquid–solid contact and culminates in substantial deterioration of heat removal from the wall. Depending on impact momentum, the drop may bounce, break up, or roll on the wall, further complicating the heat transfer process.

1.3. Regimes after impact

1.3.1. Heat transfer perspective

Clearly, wall temperature plays a crucial role in the study of drop impingement on a heated wall, influencing both impact dynamics and heat transfer performance. Based on evaporation lifetime of a single drop at different wall temperatures, four distinct evaporation regimes can be clearly identified: *film evaporation*, *nucleate boiling*, *transition boiling*, and *film boiling* [17,18], as shown in Fig. 1. The Leidenfrost point is especially important, resulting in the longest evaporation time [19]. Because of drastic differences among the four evaporation regimes, efforts have been made to quantify transition boundaries between regimes using both hydrodynamic and heat transfer considerations [20].

Bernardin et al. [21] pointed out that T_w and the impact Weber number,

$$We = \frac{\rho_f v_{drop}^2 d_{drop}}{\sigma}, \tag{1}$$

are the two most important parameters governing impact behavior and heat transfer. They provided comprehensive maps covering both impact dynamics and heat transfer regimes for low and high Weber numbers (We = 20, 60, and 220). Later, Bernardin et al. [22] also incorporated the influences of surface roughness in their maps. They reported that surface features influence boiling regimes in two major ways: (a) inducing breakup of the spread film at high wall

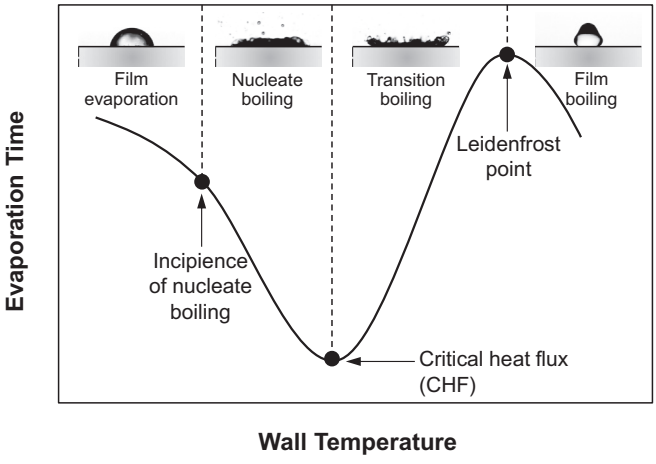

Fig. 1. Heat transfer regimes associated with a drop impinging a hot wall.

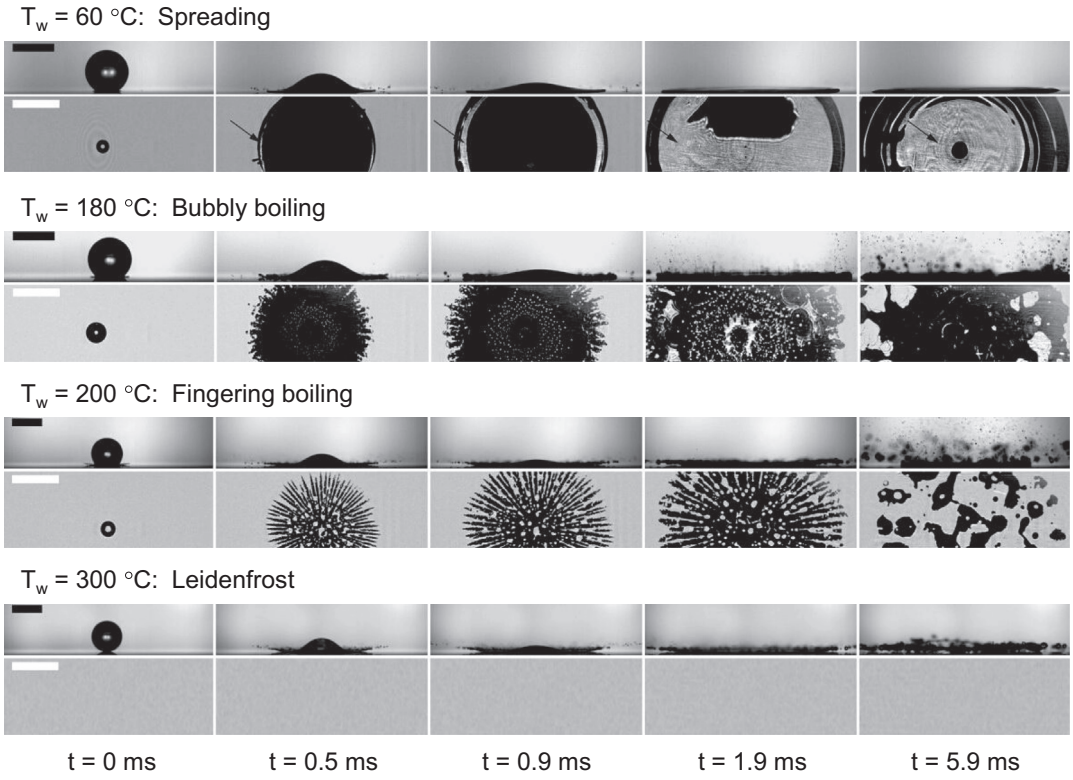

Fig. 2. Series of side-view and bottom-view snapshots of ethanol drop impinging a heated wall at *We* = 481 for different wall temperatures. Scale bars indicate 2 mm. Adapted from Khavari et al. [24].

temperatures corresponding to film boiling and high-temperature region of transition boiling, and (b) increasing nucleation site density at lower wall temperatures corresponding to nucleate boiling and lower temperature region of transition boiling.

1.3.2. Hydrodynamic perspective

Other classifications of drop impingement on a heated wall have been based mostly on observations of hydrodynamic behavior associated with the impact. Using experimental observations, Wang et al. [20,23] classified drop impingement on a heated wall into five different impact patterns: *completely wet*, *wet film boiling*, *transition*, *dry rebound*, and *satellite dry rebound*, where dry impact implies that no liquid–solid contact occurs during the impact process. They also found that *We* has stronger influence on dry wall impact than that on wet wall impact. As shown in Fig. 2, Khavari et al. [24] divided boiling behavior into four regimes: *spreading regime*, *bubbly boiling regime*, *fingering boiling regime*, and *Leidenfrost regime*. The spreading regime was described as having negligible heating effects. The fingering boiling regime was described as incurring gradual decrease in wetted area with increasing wall temperature, independence of wetted area from *We*, and vapor transport between liquid fingers.

Tran et al. [25] observed three different regimes for $T_w > T_{sat}$: *contact boiling*, where the drop boils immediately upon contact with the heated wall, *gentle film boiling*, where the drop forms a Leidenfrost vapor layer along its underside and bounces without surface contact, and *spraying film boiling*, where the drop also forms a Leidenfrost layer but shatters by ejecting tiny droplets away from the wall. Fig. 3 shows the three regimes in a T_w versus *We* plane. Recently, Staat et al. [26] measured the wetted area during drop boiling using interferometric high-speed imaging, and identified four different regimes: *deposition*, *contact-splash*, *bounce*, and *film-splash*, as shown in Fig. 4. They also identified two transition lines, one towards splashing, corresponding to increasing *We*, and another towards Leidenfrost state for increasing T_w. Castanet et al. [27] observed three regimes: *rebound*, *splashing*, and *deposition* of liquid film, which they mapped by plotting dimensionless temperature $(T_w - T_{sat})/(T_L - T_{sat})$ against the threshold parameter $WeOh^{-0.4}$ for splashing [28], where *Oh* is the Ohnesorge number defined as

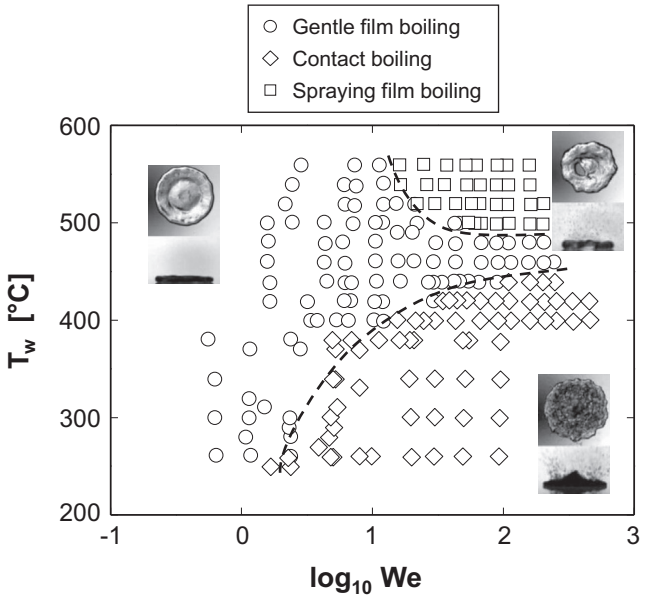

Fig. 3. Boiling regimes associated with water and FC-72 drop impact with a heated wall. Adapted from Tran et al. [25].

$$Oh = \frac{\mu_f}{\sqrt{\rho_f \sigma d_{drop}}}. \quad (2)$$

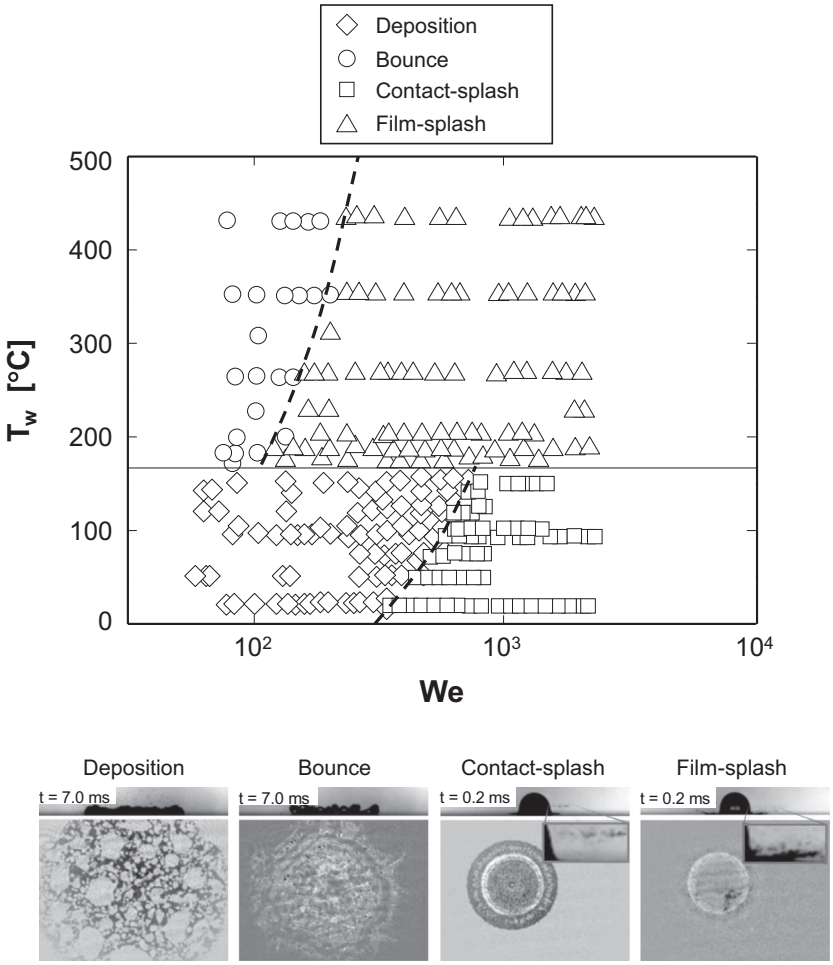

Fig. 4. Regime diagram for ethanol drop impinging a heated sapphire wall, based on outcome of impact. Adapted from Staat et al. [26].

Kandlikar et al. [29] identified four regimes: levitation after several advance and recoil cycles, levitation after first recoil, disintegration after first recoil, and disintegration after impact.

Recently, Shirota et al. [30] and van Limbeek et al. [31] used a total internal reflection technique to visualize wetting dynamics of a drop impinging a heated wall, and identified three regimes: *distinguished elaborate contact boiling*, *transition boiling*, and *Leidenfrost boiling*. They concluded that, when impact time scale (d_{drop}/v_{drop}) is on the order of the thermal time scale ($k_w\rho_w c_w/h^2$) or larger, where h is the heat transfer coefficient, the effects of heat transfer on impact behavior cannot be neglected, and the drop will make direct contact with the wall. On the other hand, when thermal time scale is longer than impact time scale, the wall remains essentially isothermal, and the impact is unaffected by heat transfer. The authors of the present study observed that boiling phenomena near the Leidenfrost point can be classified into *reflection rebound*, *explosive rebound,* and *explosive detachment* [32].

Due to rapid advances in high-speed imaging and development of increasingly more sophisticated diagnostics techniques, it is believed that new details of liquid–solid impact will emerge in future studies, which should also lead to more accurate regime identification. Given the differences between regimes identified by different researchers, this study will review published literatures using the classification based on the four regimes depicted in Fig. 1. Fig. 5 is used as a guide for defining drop parameters, and liquid, gas, and solid wall properties, and also provides simple schematics representing the extreme temperature regimes of film evaporation and film boiling.

1.4. Objectives of review

This paper is the second in a series of three review articles by the authors addressing the complex transport phenomena associated with liquid drop impact. The first reviewed fluid mechanics mechanisms of liquid drop impact on a liquid film [33]. The present study will review published articles addressing liquid drop impact on a heated wall. The third and future article will address the more practical, albeit far more complex problem of spray cooling, which involves the collective contributions of many drops impacting a heated wall.

In the present article, various aspects of drop impact on a heated wall will be reviewed in terms of interfacial behavior following the impact, as well as temporal and spatial variations of wall temperature and wall heat flux for four different heat transfer regimes: evaporation, nucleate boiling, transition boiling, and film boiling. Depictions of impact behavior by different investigators corresponding to each regime will be reviewed in terms of dominant hydrodynamic and heat transfer mechanisms, and predictive correlations and/or models.

2. Film evaporation

2.1. Modeling of heat transfer behavior

2.1.1. Modeling efforts

Film evaporation takes place when $T_w < T_{sat}$, and even when $T_w > T_{sat}$ but with the wall superheat insufficient to initiate bubble

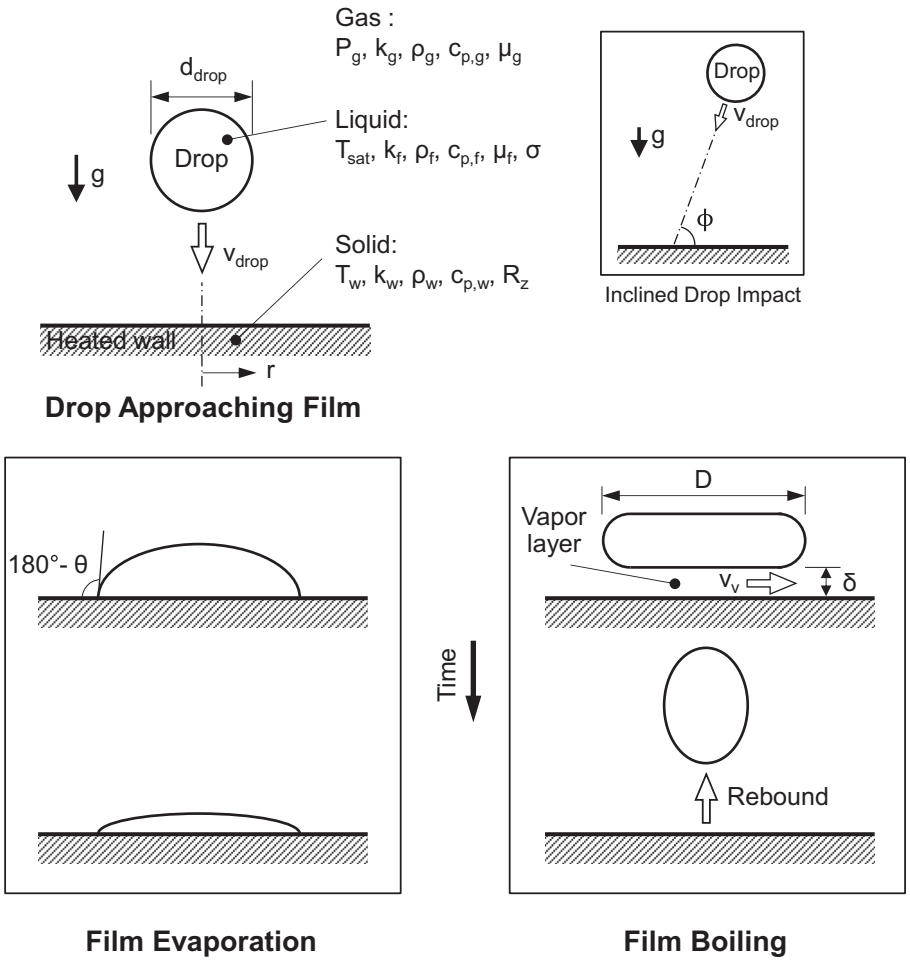

Fig. 5. Nomenclature used in drop impingement on a heated wall along with schematics for extreme temperature regimes of film evaporation and film boiling.

nucleation. Shown in Fig. 5 is a schematic representation of film evaporation, where the liquid drop spreads on the wall upon impact, and begins thinning due to evaporation. This simple depiction does not capture all possible film evaporation patterns, such as liquid receding and bouncing effects for certain conditions.

In general, drop heat transfer in the film evaporation regime is influenced by temperature variations inside the drop and the wall, wall heat flux, and drop evaporation time. di Marzo and Evans [34] proposed a model to predict the rate of change of drop volume, V, and local heat flux at the liquid interface, q'', associated with drop impact based on the assumptions of uniform wall temperature (for high thermal conductivity wall materials), and vapor phase generated only along the liquid–vapor interface,

$$-\frac{dV}{dt} = \frac{1.248\ \pi\ R^2 h_c}{\rho_w\ c_{p,g}} \left(\frac{\varepsilon}{\alpha_g}\right)^{2/3} \int_0^1 \left(\frac{x_i - x_g}{1 - x_i}\right) \left(\frac{r}{R}\right)\ d\left(\frac{r}{R}\right), \tag{3a}$$

and

$$q'' = 0.624\ h_c \left(\frac{h_{fg}}{c_{p,g}}\right) \left(\frac{\varepsilon}{\alpha_g}\right)^{2/3} \left(\frac{x_i - x_g}{1 - x_i}\right), \tag{3b}$$

where ε is the mass diffusivity and x the molar fraction. They found that spatial distribution of liquid–vapor heat flux is governed by drop dynamics [35], and heat flux is non-uniform relative to both time and space, and is higher at the outer edge due to reduced film thickness. With time, the spatially averaged heat flux increases but its radial distribution becomes more uniform. For solid walls with low thermal conductivity, di Marzo et al. [36] formulated a coupled model to tackle heat transfer in both the drop and solid wall. They also suggested using a constant spatially and temporally averaged heat flux to predict the spatial distribution of wall temperature, and attributed convective fluid motion within the drop to interaction between buoyancy and thermocapillary convection.

Ruiz and Black [37] modeled the effects of thermocapillary convection into film evaporation, which is the result of instability due to surface tension gradients at the drop's free surface. By comparing their predictions with those of a model based on heat conduction with no internal fluid motion, they proved that thermocapillary convection provides vastly different temperature distribution inside the drop, with the heat conduction model underestimating the rate of change of drop mass and drop evaporation time. Berberović et al. [38] developed a computational model to account for air motion around the liquid drop, and predicted the formation of small air bubbles in the initial impact region, which provides more realistic insight into the ensuing heat transfer. Their results showed weak dependence of the amount of heat removed from the heated wall on spatial temperature distribution at the liquid–solid interface. Strotos et al. [39] reported that internal motion induced within the drop hastens liquid mixing and helps achieve more uniform temperature within the drop, effects of which were not observed when accounting for heat conduction alone. Zhang and Gogos [40] suggested higher wall temperature can enhance uniformity of drop interface temperature.

2.1.2. Overall heat transfer

Regarding spatially averaged heat transfer in film evaporation, Chandra et al. [41] conducted experimental and modeling work

to investigate the influence of contact angle on drop evaporation rate. They reported that reducing contact angle with the aid of surfactant increases drop evaporation rate by both increasing drop-wall contact area and decreasing film thickness, and decreasing initial contact angle from 90° to 20° reduces drop evaporation time by about 50%. Wall temperature is lowest at the impact point and increases in the radial direction. Similar trends were confirmed with numerical simulations by Pasandideh-Fard et al. [12], who also found that increasing drop impact velocity enhances the spatially averaged heat flux from the wall by only a small amount, mainly because of increased liquid–solid contact area. Guo et al. [42] showed numerically that higher impact velocity causes evaporation to commence earlier, but decreases evaporation rate. On the other hand, Liang et al. [43] showed experimentally that impact velocity has only minor influence on the drop's film evaporation, and reported that evaporation rate and average heat flux increase linearly with increasing T_w. They also observed formation of several tiny bubbles at the liquid–solid interface inside the drop, which they attributed to initial gas entrainment. Theoretical work by Fukai et al. [44] suggested that drop diameter and height depend more strongly on T_w in the recoiling stage more than in the spreading stage.

2.1.3. Local heat transfer effects

A few investigators have focused their efforts on localized heat transfer effects in the drop. Cui et al. [45] experimentally investigated the effects of dissolved gas and solid salts on evaporation heat transfer. Dissolved salts were found to reduce evaporation rate by decreasing water vapor pressure. But dissolved gas has the opposite effect, enhancing evaporation by coming out of solution to form bubbles in the liquid. An important highlight from their work is the observation of small salt crystals precipitating along the edges of the liquid cap, which is proof that the evaporation rate is highest at the triple-phase (liquid–gas–solid) contact line. Nakoryakov et al. [46] also arrived at the same conclusion concerning the triple-phase line in their drop experiments. These triple-phase line observations confirm numerical predictions by several investigators, including di Marzo and Evans [34], Francois and Shyy [35], Strotos et al. [39,47], Herbert et al. [48,49], Healy et al. [50], and Ge and Fan [51]. These studies showed that, as drop motion comes to a halt, the heat transferred in the vicinity of the triple-phase contact line constitutes a considerable fraction of the total heat transfer. In their simulation work, Herbert et al. [48] estimated this fraction at about 50% of total.

2.1.4. Heat transfer enhancement

Deng and Gomez [52] found that electrically charged ethanol drops undergo faster evaporation due to reduced contact angle. Srikar et al. [53] and Weickgenannt et al. [54] found that covering the surface with a electrospun nanofiber mat, which is water permeable, can enhance heat transfer during impact by eliminating drop receding and bouncing effects. Manzello and Yang [55] investigated water drop impingement on a heated wax wall. A low *We* drop was observed to recoil much faster with increasing T_w, while a high *We* drop was found to incur instabilities along the periphery of the spreading liquid film. Manzello and Yang [56] also noted that evaporation rate can be hastened by adding 30% sodium acetate trihydrate in the water.

Surface texturing is another means for influencing drop impact and heat transfer. Alizadeh et al. [57] reported that impact dynamics are weakly dependent on T_w for textured superhydrophobic surfaces. Moon et al. [58] showed that heat transfer effectiveness increases with increasing *We*, but this dependence is also influenced by wetting characteristics, and, in the case of total wetting, heat transfer effectiveness at higher texture area fraction is higher than that at lower texture area fraction.

2.2. Contact temperature

In 1978, Seki et al. [59] measured transient liquid–solid 'contact temperature', $T_{contact}$, using a thin-film thermometer, and compared measurements to theoretical value that accounts for temperatures as well as heat diffusion properties of both liquid and solid wall,

$$T_{contact} = \frac{T_w\sqrt{(k\rho c_p)_w} + T_f\sqrt{(k\rho c_p)_f}}{\sqrt{(k\rho c_p)_w} + \sqrt{(k\rho c_p)_f}}. \quad (4)$$

The theoretical contact temperature determined from Eq. (4) is constant during the transient associated with liquid contact with the wall, and satisfies the condition $T_w > T_{contact} > T_f$. However, the value of $T_{contact}$ is biased towards that of the medium with the larger product $(k\rho c_p)$. For most situations involving a drop impinging a heated wall, $(k\rho c_p)_w \gg (k\rho c_p)_f$, which results in $T_{contact} \cong T_w$. Seki et al. found that T_w drops to $T_{contact}$ immediately after the initial drop contact, and $T_{contact}$ increases with increasing initial wall temperature. They determined that $T_{contact}$ for a water drop is approximately constant for $100 \leqslant T_w - T_{sat} \leqslant 200$ °C, but increases again for $T_w - T_{sat} \geqslant 200$ °C, where the 200 °C temperature difference roughly coincides with the Leidenfrost point, where liquid–solid contract is no longer prevalent. Fig. 6 shows variations of measured contact temperature with T_w for water and ethanol drops, along with theoretical values determined from Eq. (4). The water data agree well with the theoretical values for $T_w - T_{sat} \leqslant 100$ °C, while good agreement is achieved for all temperatures for ethanol. This proves the effectiveness of Eq. (4) for determination of the contact temperature.

Using transparent-to-infrared wall material, Tarozzi et al. [60] developed a non-intrusive optical method to measure $T_{contact}$ from the underside of the impact surface. The wall was coated atop with a very thin layer of high emissivity opaque paint to respond effectively to an infrared camera located beneath. Bhardwaj et al. [61] adopted a novel laser-based $T_{contact}$ measurement technique, which had temporal and spatial resolutions of 1 μs and 15 μm, respectively. They also used numerical methods to confirm the feasibility of this technique.

2.3. Contact angle

Bernardin et al. [62] summarized the different types of contact angle commonly reported in the literatures, and investigated the temperature dependence of quasi-static advancing contact angle, θ, for a water drop on a polished aluminum surface. Their experiments spanned wall temperature and pressure ranges of 25–170 °C and 101.3–827.4 kPa, respectively. While no pressure

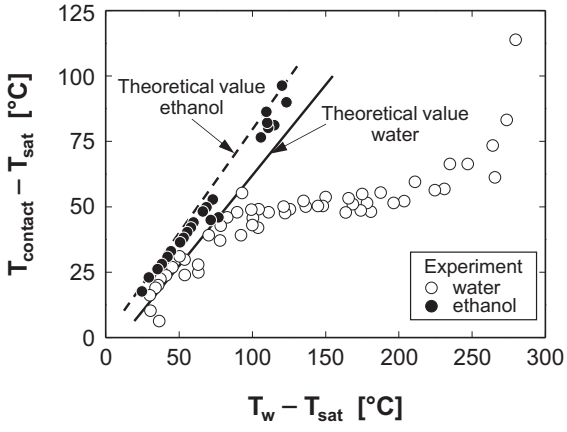

Fig. 6. Contact temperature versus initial wall temperature for water and ethanol drops. Adapted from Seki et al. [59].

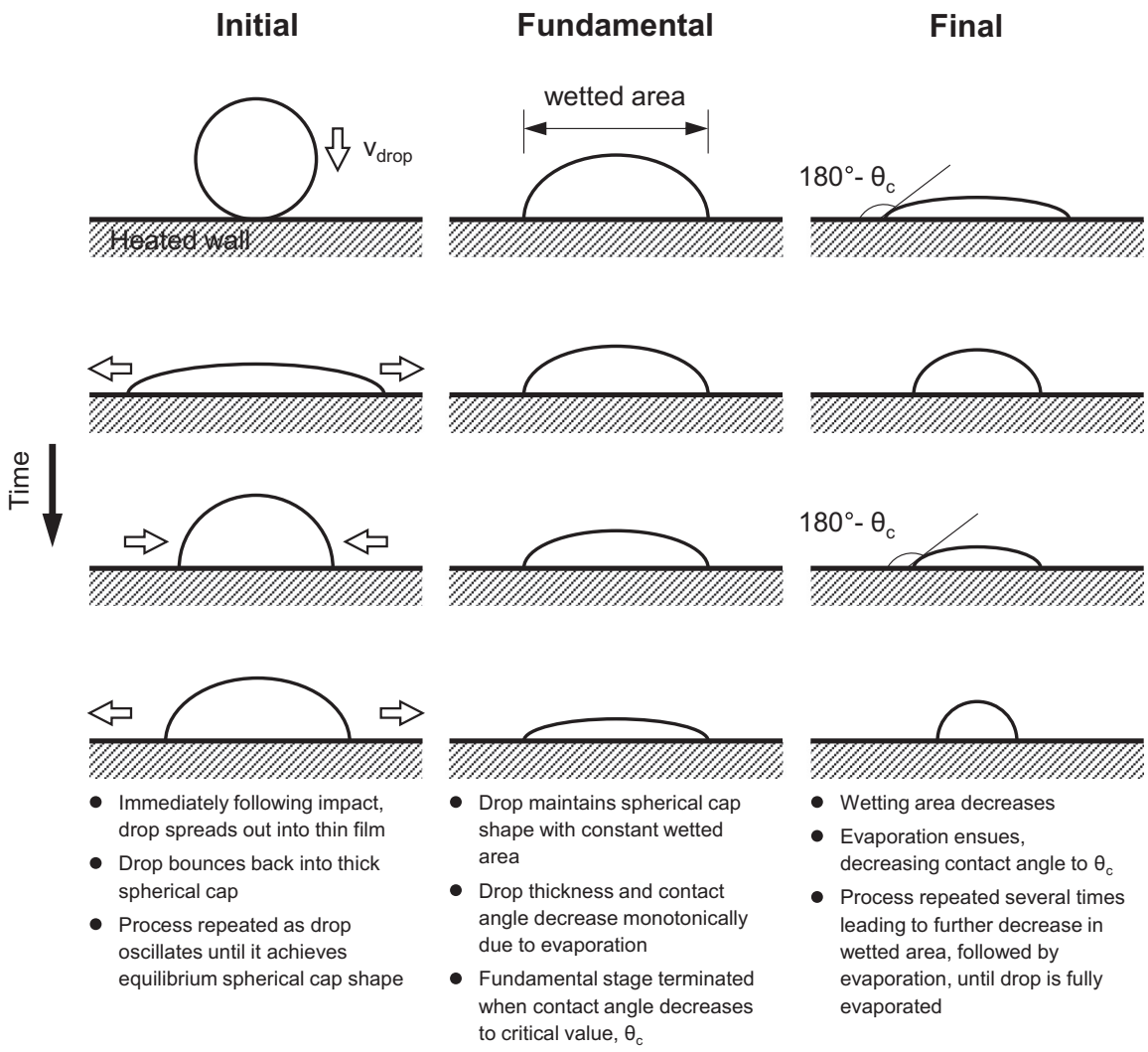

Fig. 7. Schematic representation of three stages of drop impact with a heated wall during film evaporation regime.

effects were observed, two distinct temperature-dependent regimes were identified: a low temperature regime, $T_w < 120$ °C, where contact angle is fairly constant at $\theta = 90°$, and a high temperature regime, $T_w > 120$ °C, where contact angle decreases fairly linearly towards zero, according to the relation

$$\theta = 157.4 - 0.55\,T_w, \tag{5}$$

where θ and T_w are expressed in degrees and °C, respectively. Kandlikar and Steinke [63] noted that the dynamic receding contact angle for water impinging on a heated stainless steel or copper wall increases to the same value as the dynamic advancing contact angle for T_w = 135–150 °C. Kandlikar and Steinke [64] also found that the dynamic advancing contact angle extends the equilibrium advancing and receding contact angles during interface motion. Moon et al. [65] observed that dynamic contact angles for Newtonian and non-Newtonian drops are almost equal during liquid spreading, but, during recession, contact angle changes substantially with temperature because of the strong dependence of viscosity on temperature.

2.4. Evaporation stages

2.4.1. Major classifications

As discussed earlier, Fig. 5 provides a simple depiction of film evaporation. Discussed in this section are detailed depictions of the same process.

It is commonly accepted that film evaporation can be divided into three stages [45,66–71]: initial, fundamental, and final, as illustrated in Fig. 7. The initial stage refers to the drop impingement phase, where, following contact, the drop spreads and oscillates until it achieves equilibrium state consisting of a spherical liquid cap. The fundamental stage refers to evaporation of the spherical cap, while preserving constant wetting area, but with the contact angle and drop height gradually abating. The final stage corresponds to a rapid succession of events, where the spherical cap shrinks laterally into a cap with smaller wetted area then incurs further evaporation, before shrinking again into a smaller cap and evaporating, and so on, until the liquid is completely evaporated. Rymkiewicz and Zapalowicz [68], Shen et al. [70], and di Marzo and Evans [34] showed that the fundamental stage accounts for about 80%, 60%, and 90–95%, respectively, of the total drop evaporation time. The dominance of the fundamental stage is also evidenced in a study by Bonacina et al. [72], who achieved reasonable agreement with experimental heat transfer measurements using an analytical model based on the assumption of constant wetted area over the entire evaporation period. Additionally, Sodtke et al. [73] reported that the diameter of the wetted area decreases by only 5% during the first 85% of the drop evaporation time. Shen et al. [70] showed that the final stage accounts for only 30% of the evaporation time. It should be mentioned that several investigators [34,36,67,74] assumed that the

liquid cap maintains a constant receding contact angle during the final stage.

Lee et al. [74] used an alternative heat transfer approach to classify drop evaporation. He recommended a two-part process: a first part, characterized by transient fluctuations in the heat transfer coefficient, and a second part, in which the heat transfer coefficient is constant. Their measurements revealed that transient fluctuations in the heat transfer coefficient during the first part are not the result of transient conduction alone, but are also influenced by drop deformation dynamics and vapor behavior near the impact site. The second part is consistent with the third stage and constant receding contact angle in the three-stage classification discussed in the previous paragraph. Lee et al. constructed a model for each part, and derived separate relations for evaporation time for the two parts:

$$\text{First part}: \quad t_e = \frac{\rho_f h_{fg} d_{drop}}{4h(T_w - T_g)} \left[\tan(\theta_0/2) - \tan(\theta_r/2) + \frac{1}{3}\{\tan^3(\theta_0/2) - \tan^3(\theta_r/2)\}\right], \tag{6a}$$

$$\text{Second part}: \quad t_e = \frac{\rho_f h_{fg} d_{drop}}{2h(T_w - T_g)} \left\{\frac{(1-\cos\theta_r)^2(2+\cos\theta_r)}{\sin^3\theta_r}\right\}, \tag{6b}$$

where T_g, h, θ_0, and θ_r are ambient temperature, heat transfer coefficient, initial contact angle, and receding contact angle, respectively.

2.4.2. Critical contact angle

As discussed in the previous section, receding contact angle marks the transition from the fundamental stage to the final stage of drop evaporation. Specifically, when the liquid–solid contact angle falls below a specific receding contact angle termed *critical contact angle*, it will no longer be possible to maintain the constant wetting area prevalent in the fundamental stage. Qiao and Chandra [67] estimated the critical contact angle at 10° for a water drop on a stainless steel wall. Shen et al. [70] reported similar critical contact angle values for water on polished silicon, nanostructured silicon, and thin gold layered silicon. On the other hand, Hu and Larson [66] and Liang et al. [43] came out with critical contact angle estimates of 2–4° for water on glass, and 5–8° for water on stainless steel, respectively. And images captured by Guilizzoni and Sotgia [75] indicate that a water drop on a smooth brass surface will maintain constant wetting area even at a contact angle of 4°. A noteworthy finding from the study by Qiao and Chandra is that the receding contact angle is not influenced by surfactants.

It should be emphasized that all studies mentioned in the above paragraph are based on experiments using water drops. Liang et al. [43] emphasized that the three stages of film evaporation, as discussed above, are water specific, and not valid for all fluids. This is evident from absence of a constant area stage in experiments with butanol and ethanol, where both wetting area and drop height decrease monotonically throughout the evaporation process. They attributed these differences in evaporation behavior to large differences in surface tension of these two fluids compared to water.

Experiments by Li et al. [76] with water drops on a polished wall revealed that the height of recoiling drop increases with increasing T_w, which was attributed to Marangoni flow induced by surface tension gradients resulting from surface temperature gradients in the liquid film. Sefiane et al. [77] showed that ethanol–water mixtures display evaporation stages that combine those of pure water and pure ethanol, including an initial stage of constant wetting area, followed by a stage where contact angle and wetting area decrease simultaneously. However, more studies are needed to further investigate the different stages of evaporation for different fluids, fluid mixtures, wall materials and textures, wall temperatures, and operating pressures.

3. Nucleate boiling

3.1. Nucleate boiling heat transfer

The nucleate boiling region extends from the onset of boiling, which occurs at a wall temperature slightly above T_{sat}, to the critical heat flux (CHF) point, which corresponds to shortest drop lifetime as shown earlier in Fig. 1. Tarozzi et al. [60] and Tartarini et al. [78] reported that predicting the onset of boiling requires accurate measurement of $T_{contact.}$, and that bubbles begin to nucleate within the bottom of the drop when $T_{contact}$ exceeds T_{sat}.

Cui et al. [45] investigated the effects of dissolved gas and salts on nucleate boiling in the drop. They reported that dissolved carbon dioxide enhances heat transfer by a small amount. Dissolving sodium carbonate in the liquid was observed to inhibit bubble coalescence in the liquid and promote foaming, which reduces drop lifetime. Dissolved sodium bicarbonate reduces drop lifetime even more than sodium carbonate, because it decomposes when heated to produce carbon dioxide, further augmenting bubble formation. Salt particles coming out of solution and precipitating inside the drop during evaporation were observed to augment bubble nucleation.

Influences of parameters such as drop volume, wall material and thickness, surface tension, and use of surfactants, on nucleate boiling have been assessed by several investigators. Nakoryakov et al. [46] reported that drop evaporation time decreases with decreasing drop volume or increasing wall thickness; they attributed the latter to slower heat removal from thick compared to thin walls. Longer drop lifetime was measured for a stainless steel wall compared to a copper wall, mainly due to lower thermal diffusivity of stainless steel, and decreasing wall thickness delays CHF. Qiao and Chandra [67] showed that adding 100–1000 ppm surfactant in a water drop increases drop-wall contact area and promotes bubble nucleation, however drop lifetime is greatly reduced because of the foaming produced. Okawa et al. [79] showed how dispersing nanometer-sized titanium-dioxide particles in the water drop to produce a nanofluid yields substantial improvement in nucleate boiling heat transfer at low wall superheat, which is resulted from increased contact area. However, heat transfer is degraded at high superheat because fast vaporization during the initial stage of impact reduces liquid–solid contact area in the later stages. Xiong and Yuen [80] found that maximum heat transfer rate occurs at a wall superheat of 50–60 °C for pure liquids, and this superheat value is independent of drop size for fuel drops, but decreases slightly with increasing drop size for water drops. Moita and Moreira [81] found that drops with smaller surface tension and latent heat are more likely to undergo faster boiling, which promotes breakup of liquid drops and generation of dry surface areas, compromising cooling performance.

Bernardin and Mudawar [82] reported that interference resulting from a drop impinging on top of another spreading drop or from lateral collision of neighboring drops, reduces effective liquid–solid contact area and corresponding heat transfer rate compared to isolated drops. Chen and Hsu [83] developed a microthermocouple probe to measure transient temperature of the solid wall after drop impact, which they used to determine transient heat flux in the liquid contact area. Fig. 8 shows average heat flux of water drops at atmospheric pressure ranges from 10^5 to 10^7 W/m^2, corresponding to wall superheat values from 50 to 450 °C, which extend beyond just the nucleate boiling region. Park et al. [84] showed that the total amount of heat transferred during the entire impact process per water drop volume for $110 < T_w < 210$ °C ranges from 0.028 to 0.048 J/mm^3. For successive drop impact, Park et al. [85] showed that nearly all water drops vaporize for $100 < T_w < 150$ °C, while, for $150 < T_w < 220$ °C, heat

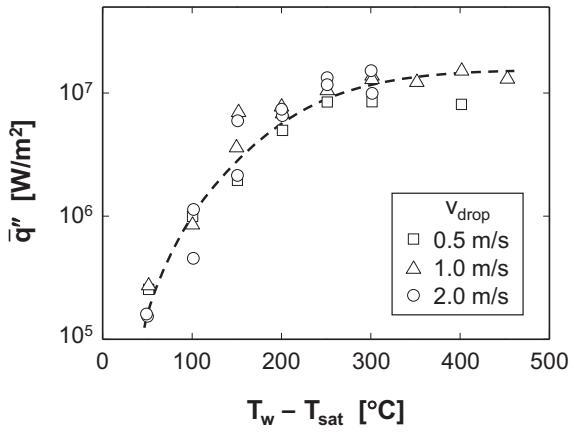

Fig. 8. Average heat flux during water drop impact on an Inconel wall with nickel coating. Adapted from Chen and Hsu [83].

transfer is compromised by drop shattering. Despite these useful findings, the complex phenomena associated with either vertical or lateral multi-drop interference, and their importance to spray cooling, warrant significant additional study.

3.2. Critical heat flux

Kandlikar and Steinke [63] reported that CHF in impinging drops is caused by motion of the liquid–vapor interface due to a thin vapor layer they captured using side-view high-speed video imaging of the liquid–vapor interface and liquid–solid–vapor contact line [86]. Bernardin et al. [21,22] showed that CHF in water drops occurs at $T_w = 130$ °C, regardless of impact velocity, surface roughness, or impact frequency. However, McGinnis and Holman [87] showed that heat transfer rate per drop exhibits a maximum at $T_w > 149$ °C. They correlated data for maximum heat transfer rate, Q_{max}, for water, acetone, and alcohol drops according to the relation

$$\frac{Q_{max}}{\rho_f\, d_{drop}^3\, h_{fg}^*} = 8.44\times10^{-4}\left(\frac{\rho_f^2\, v_{drop}^2\, d_{drop}}{\rho_g\, \sigma}\right)^{0.341}, \tag{7}$$

where h_{fg}^* is the modified latent heat given by

$$h_{fg}^* = h_{fg} + c_{p,f}\frac{T_w - T_{sat}}{2}. \tag{8}$$

For inclined impact, consisting of a drop impacting the wall at angle ϕ between the flow axis and the wall, the maximum heat transfer rate given by Eq. (7) should be multiplied by $0.82(\sin\phi)^{0.682}$ to account for the normal velocity component. In follow-up work, Holman et al. [88] extended their results to smaller drops, including data for R11 and R113, and recommended the following correlation:

$$\frac{Q_{max}}{\rho_f\, d_{drop}^3\, h_{fg}^*} = 18.5\times10^{-4}\left(\frac{\rho_f\, v_{drop}^2\, d_{drop}}{\rho_g\, \sigma}\right)^{0.341}. \tag{9}$$

Okawa et al. [79] increased CHF by about 50% by dispersing nanoparticles in the water drop. On the other hand, Duursma et al. [89] showed that nanoparticles in water drops do not produce noticeable enhancement in heat flux, but increasing *We* does increase CHF. Akhtar et al. [90] identified three different impact and deformation patterns for a water drop impinging a heated stainless steel wall near CHF ($140 < T_w < 160$ °C): *drop adhesion* for $We < 15 \pm 5$, *drop spread without atomization* (until complete evaporation) for $20 \pm 5 < We < 300 \pm 20$, and *drop breakup* for $We > 350$.

Overall, research on CHF is far from complete, both in terms of modeling and experiment, especially considering the discrepancies among investigators. These discrepancies might be related to the relatively large number of parameters influencing CHF.

3.3. Bubbles and secondary droplets

3.3.1. Bubble behavior

Liang et al. [43], Moita et al. [91], Mehdizadeh and Chandra [92], and Fujimoto et al. [93] all reported that a single bubble or circular bubble rings are formed in the drop immediately after impact, which they attributed to air entrapment between the drop and the wall, independent of thermal effects. Subsequently, vapor bubbles are formed around the initial air bubbles [93]. Thereafter, isolated vapor bubbles are formed in the rim of the spreading liquid film, which are the result of boiling of the liquid.

Few investigators combine nucleate and transition boiling, addressing them collectively as *bubble boiling* [94,95]. Chaves et al. [96] observed bubble formation in the bubble boiling regime with ethanol drops, and concluded that maximum spreading diameter and bubble lifetime depend on *We* and T_w, and higher *We* decreases film thickness and corresponding size of bubbles growing in the spreading liquid film.

3.3.2. Secondary atomization

Cossali et al. [95] performed experiments to capture thermally induced secondary droplet atomization. As shown in Fig. 9, growth and rupture of vapor bubbles in the bubble boiling regime produce a large number of small secondary droplets, and increasing impact velocity slightly decreases droplet size, while surface roughness has a relatively weak influence on bubble formation. In another study [94], they showed that the influence of liquid viscosity is fairly insignificant, and reported that secondary droplets in the bubble boiling regime are always rejected normal to the heated wall as depicted in Fig. 9. Qiao and Chandra [97] showed experimentally that nucleate boiling of drops is not affected by reduced gravity, evidenced by vapor bubbles nucleating on the solid wall then rising into the liquid even in the absence of gravity.

Chaves et al. [96] proposed a mechanism for secondary droplet formation in the bubble boiling regime: breakup of thin jets caused by explosion of vapor bubbles through the liquid lamella. With increasing T_w, both the jet length and number of secondary droplets increase. Liang et al. [43] and Cossali et al. [94,95] provided experimental evidence supporting this mechanism as shown in Fig. 10(a), however, they also captured another mechanism for formation of tiny droplets: jets ejected atop pagoda-like bubbles, as shown in Fig. 10(b). Moita and Moreira [98] also observed this pagoda-like bubble mechanism. Liang et al. [43] suggested that pagoda-like bubbles emerge in the thick portions of the spreading film, then push the liquid upwards by high pressure inside the bubble.

Moita and Moreira [99] proposed the following correlation for time-averaged Sauter Mean Diameter (SMD) of secondary droplets, d_{32}, in the nucleate boiling regime:

$$\frac{d_{32}}{d_{drop}} = CWe^{-0.14}Re^{-0.11}Ja^{-0.3}, \tag{10}$$

where C is an empirical parameter, Re the Reynolds number defined as $Re = \rho_f\, v_{drop} d_{drop}/\mu_f$, and Ja the Jacob number defined as $Ja = c_{p,f}(T_w - T_{sat})/h_{fg}$. Moita and Moreira also suggested that secondary droplet formation in the nucleate boiling regime is the outcome of a thermally-induced mechanism associated with increased vapor pressure in bubble nucleation sites, combined with surface tension effects.

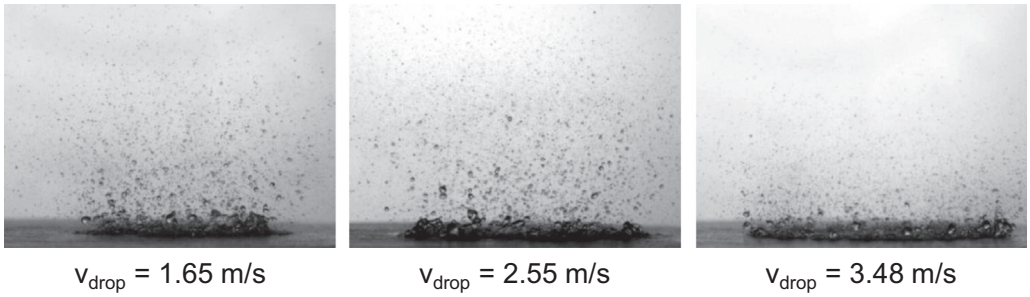

Fig. 9. Secondary atomization in nucleate boiling of water drop impacting an aluminum alloy wall for T_w = 145 °C and $\tau = v_{drop}\, t/d_{drop}$ = 6. Adapted from Cossali et al. [94].

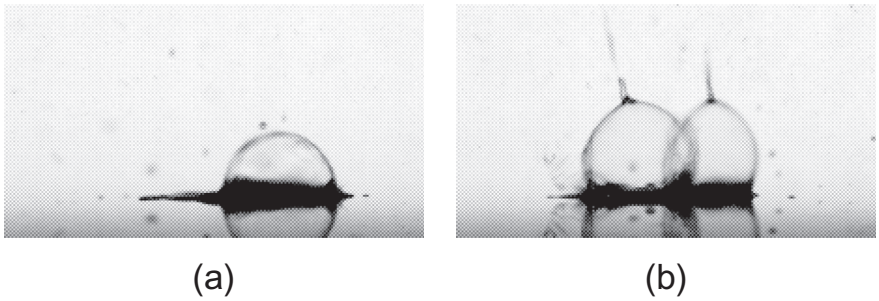

Fig. 10. (a) Plain bubbles, and (b) pagoda-like bubbles in the bubble boiling regime (combined nucleate and transition boiling) for a water drop impacting a stainless steel wall at *We* = 10 for T_w = 220 °C. Adapted from Liang et al. [43].

4. Transition boiling

Transition boiling spans the region between the CHF and Leidenfrost points. A major challenge in pinpointing and characterizing the film boiling regime is that these two important end points are not yet accurately determined. This is one reason why publications addressing the transition boiling regime are quite sparse.

Akhtar et al. [90] derived the following correlation for maximum spreading diameter, D_{max}, of the drop during transition boiling:

$$D^*_{max} = \frac{D_{max}}{d_{drop}} = 0.003\, We + 3.21, \tag{11}$$

which is valid for $160 < T_w < 200$ °C and $100 < We < 650$. Chandra and Avedisian [100] found that wetting evolution and drop spreading rate for heptane are independent of T_w in the early stage of impact, because of negligible surface tension or viscous forces. They also reported that heptane drops impinging a porous wall do not transit to film boiling at T_w = 200 °C, which is quite different from impingement on a stainless steel wall. Nikolopoulos et al. [101] showed numerically the existence of a circular vortex ring of air inside the drop, and that bubble size in the transition boiling regime increases with increasing T_w. However, their model does not account for heat transfer in the wall.

In their study of interactions between drops during impingement of a liquid drop train, Qiu et al. [102] found that splashing angle (*i.e.*, angle between splashed liquid sheet and the wall) decreases as T_w is increased from transition boiling to film boiling. They also reported that, once splashing is complete, the size, velocity, and direction of splashed secondary droplets acquire bell-shaped distributions relative to different frames.

5. Film boiling

5.1. Leidenfrost point

5.1.1. Static Leidenfrost point

Historically, film boiling of a liquid drop impinging a heated wall has been termed the Leidenfrost phenomenon after J.G. Leidenfrost, who published his pioneering article on this topic in 1756 [103], and is associated with formation of a very thin vapor layer between the drop and the wall [104]. Burton et al. [105] showed that this vapor layer forms a concave depression in the drop interface facing the wall whose precise shape is dictated by drop size, independent of T_w.

In present day literatures, a specific Leidenfrost temperature, T_L, is identified as the lowest wall temperature of the film boiling regime, and has been investigated mostly in conjunction with sessile rather than impinging liquid drops [19,21,80,106]. In general, two different methods have been adopted to determine T_L [107]: thermodynamic and hydrodynamic. The thermodynamic method defines T_L as the wall temperature at which total evaporation time of the drop is longest, while the hydrodynamic method relies on temperature measurements to determine when a stable vapor layer begins to form between the drop and the wall. To distinguish Leidenfrost phenomena associated with sessile versus impinging drops, T_L is used in the present study to denote the *static Leidenfrost point* associated with sessile drops, which will be reviewed briefly first. Further details concerning the sessile drop Leidenfrost phenomenon, including evolution of drop shape, parameters, behavior of the vapor layer, and models, can be found in review articles by Quéré [108] and Brutin et al. [109].

Bernardin and Mudawar [110] provided a comprehensive review of research on T_L prior 1999, including influences of liquid mass and size, method of liquid deposition on the wall, liquid properties, liquid's initial subcooling, thermal properties of solid wall, surface finish, pressure, and impurities. They also assessed the predictive accuracy of prior models for T_L by exploring the above influences for acetone, benzene, FC-72, and water sessile drops on heated aluminum surfaces with polished, particle blasted, and rough sanded finishes. Their results suggested that liquid subcooling, dissolved gasses, and wall material only weakly influence T_L, while large-scale surface roughness has a strong influence on T_L. Overall, they concluded that prior models lack robustness, and were deemed ineffective in predicting T_L. Using experimental data from [110], Bernardin and Mudawar [111] developed a new T_L model for sessile drops, based on surface cavity characterization,

as well as bubble nucleation, growth, and interaction criteria. The premise for their model is that as T_L is approached from the nucleate boiling side, smaller and more numerous surface cavities become activated, and the growth rate of bubbles increases appreciably. For liquid–solid interface temperatures at or above T_L, a sufficient number of cavities are activated, and the bubble growth rate becomes large enough that liquid in immediate vicinity of the wall is nearly instantaneously converted to vapor upon contact. These two phenomena were deemed responsible for formation of a continuous insulating vapor layer between the liquid and the wall.

Several investigators provided detailed assessments of the influence of pressure on T_L. Testa and Nicotra [112] showed experimentally that the increase in T_L follows the same trend as T_{sat} under vacuum conditions, therefore T_L decreases with decreasing pressure. Celestini et al. [113] showed that, by decreasing the pressure, the Leidenfrost phenomenon can occur even at room temperature. By conducting experiments under high pressure, Emmerson [114] confirmed these pressure trends, and also found that T_L is independent of thermal diffusivity of the heated wall. Emmerson and Snoek [115] explored the pressure effect further by testing different fluids. For R C51-12, R113, carbon tetrachloride, and chloroform, T_L was shown to approach but not exceed the critical temperature at the critical pressure. However, T_L for water was found to increase with increasing pressure to a maximum in excess of the critical temperature, then decrease to the critical temperature as critical pressure is approached.

Another important variable whose effects on T_L were addressed by several investigators is wall roughness. Chandra and Avedisian [19] suggested that T_L is higher for rough surfaces compared to a smooth surface, and Avedisian and Koplik [116] showed that surface porosity increases T_L. Kim et al. [117,118] used custom-fabricated surfaces to demonstrate how nanoporosity is very effective at increasing T_L by initiating heterogeneous bubble nucleation during initial short-lived solid–liquid contact, which disrupts the continuous vapor layer. Kwon et al. [119] and Kruse et al. [120] found that sparse hot wall texture increases T_L via capillary wicking. Munoz et al. [121] noted that coating the heated wall with hydrophilic zeolite increases T_L. On the other hand, Arnaldo del Cerro et al. [122] found that micropatterned structures significantly decrease T_L.

Other parameters that influence T_L include surface tension and gravity. Takata et al. [123,124] showed that a decrease in contact angle decreases T_L. Qiao and Chandra [67] arrived at the same conclusion by using surfactant to decrease surface tension. On the other hand, Huang and Carey [125] showed that dissolving salt in water drops increases T_L. Maquet et al. [126] found that T_L increases with increasing gravity. Celestini and Kirstetter [127] suggested that the Leidenfrost phenomenon can be suppressed by applying an electric field between the drop and the heated wall, using a voltage above a critical value (about 40 V for a mm-scale drop). Recently, Linke et al. [128] tested ratchet-shaped surface features, which, for $T_w > T_L$, were shown to cause sessile drops to move laterally across the wall at velocities exceeding 10 cm/s; this surface enhancement technique has been widely adopted in the scientific community [129–137]. Overall, dependence of T_L on a large number of parameters has made the task of developing a universal model for T_L quite elusive.

Other studies were focused on determining precise T_L values for different fluids and wall materials. For example, Gottfried et al. [104] found that T_L is l00-105 °C above T_{sat} for all liquids except water, and the value of T_L for water depends on wall material and method of drop deposition on the wall but not on drop size, varying from 150 to 210 °C above saturation. Nagai and Nishio [138] measured T_L for acetone, cyclohexane, ethanol, Rl13, and water on single-crystal and metal plates, and showed that T_L is dictated mostly by wettability and thermal properties of the wall, and is less dependent on surface roughness. Baumeister and Simon [139] addressed the dependence of T_L on wall material. For ethanol, they measured a T_L of 178.5 °C on stainless steel, compared to 155 °C on aluminum.

5.1.2. Dynamic Leidenfrost point

In the case of a sessile drop, gravity provides the only means for promoting liquid contact with the wall [104]. While for an impinging drop, this contact is mainly the result of drop momentum, which increases the Leidenfrost temperature [140]. Because of dependence of the Leidenfrost phenomenon on impingement momentum, an alternate *dynamic Leidenfrost point* temperature, $T_{L,d}$, which is higher than T_L, was proposed by Rein [141] as the minimum wall temperature at which the developing vapor layer causes the impinging drop to bounce without shattering [25]. Xiong and Yuen [80] showed experimentally that $T_{L,d}$ is 90–120 °C above T_{sat} for liquid fuels, and 180–210 °C above T_{sat} for water.

Pedersen [142] suggested that $T_{L,d}$ can be influenced by impact velocity, while, as shown in Fig. 11, Bernardin et al. [21] showed experimentally that $T_{L,d}$ is less sensitive to impact velocity. Wang et al. [23] reported that the drop rebounds from the heated wall at $T_w < T_{L,d}$ for high impact *We*. They used spring analogy to explain this trend, suggesting that the thin vapor layer behaves as a spring, which contributes to the drop's rebound. For low *We*, dampening effects due to viscosity and surface tension weaken the spring force, which implies that a higher wall temperature is required to generate sufficient vapor pressure to strengthen the vapor layer's spring force. Celata et al. [143] investigated the effects of impact velocity and wall inclination on $T_{L,d}$, and concluded that $T_{L,d}$ decreases with increased drop velocity or decreased impact angle. Yao and Cai [144] arrived at a similar conclusion, indicating where $T_{L,d}$ decreases with decreasing impact angle. They correlated $T_{L,d}$ for water drops according to

$$T_{L,d} = T_{sat} + 135.6\, We^{0.09}\,, \tag{12}$$

where the temperatures are expressed in °C, and *We* accounts for impact momentum. They also correlated impact angle effects according to

$$\frac{T_{L,d} - T_{sat}}{T_{L,i} - T_{sat}} = 0.028\ \phi - 0.00019\ \phi^2, \tag{13}$$

where ϕ is expressed in degrees. Bertola and Sefiane [145] provided the following correlations for water and water with 200 ppm polymer additive:

$$T_{L,d} = 164.72 + 29.97\, We^{0.38}\,, \tag{14a}$$

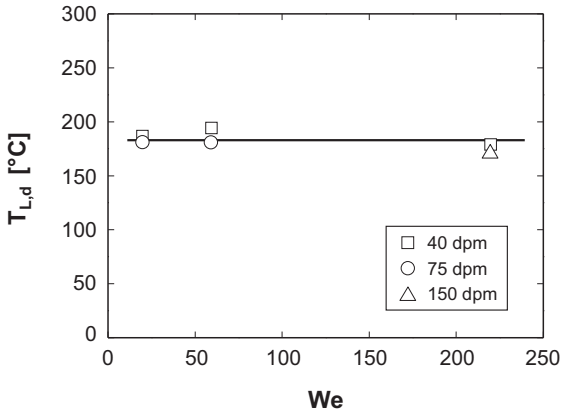

Fig. 11. Variation of dynamic Leidenfrost temperature for water drop with *We* for different drop frequencies (drops per minute). Adapted from Bernardin et al. [21].

and

$$T_{L,d} = 157.62 + 2.11\ We^{0.54}\ , \tag{14b}$$

respectively. However, they suggested that the designation 'dynamic Leidenfrost temperature' may be misleading for water with polymer additive because it would imply that the impacting drop never wets the wall, whereas wetting may occur for such fluid [146]. In works by Tran et al. [25], Shirota et al. [30], Nigmatulin et al. [147], and Karl and Frohn [148], $T_{L,i}$ was found to increase with increasing impact velocity or *We*, and this trend was attributed to shorter time available for formation of the vapor layer, which requires higher wall temperature to generate the vapor layer. However, this conclusion is opposite to that of Celata et al. [143].

Surface roughness has been suggested as one of the parameters influencing $T_{L,d}$. Pedersen [142] indicated that $T_{L,d}$ can be greatly influenced by surface roughness, but did not provide supporting experimental evidence. Later, Bernardin et al. [22] conducted a thorough investigation of surface roughness effects. For sessile drops, they suggested that sufficiently large surface roughness features penetrate the vapor layer beneath the drop, yielding higher T_L for rougher surfaces. On the other hand, surface roughness has a distinctly different influence on $T_{L,d}$ for impinging drops, where protruding roughness features tend to rupture the liquid film resulting from the impact, greatly reducing pressure beneath the drop, and therefore yielding lower $T_{L,d}$ compared to a polished surface. A similar trend was suggested by Tran et al. [149], who explained that the lateral flow of vapor generated beneath the drop is inhibited by the roughness, therefore vapor pressure needed to support the drop could be reached at lower wall temperature.

Regarding other influences, Bernardin et al. [21] and Senda et al. [150] showed that $T_{L,d}$ is independent of impact frequency, as shown earlier in Fig. 11. Weickgenannt et al. [151] showed that a mat of polymer nanofibers electrospun on the heated wall increases $T_{L,d}$ by promoting liquid penetration into the mat, which suppresses receding and bouncing behavior of the drop. Nair et al. [152] reported that carbon-nanofibers formed on the wall increase $T_{L,d}$ because they are cooled by the vapor flow prior to drop impact. Ng et al. [153] introduced a method of inducing vibrations in the heated wall to increase $T_{L,d}$ for the purpose of enhancing drop cooling efficiency.

Studies on modeling of $T_{L,d}$ are quite sparse. Bernardin and Mudawar [154] extended their sessile drop Leidenfrost model [111] to impacting drops by accounting for changes in fluid properties at the liquid–solid interface resulting from the rise in interfacial pressure created by the impact. They also revealed that the elastic impact pressure model proposed by Engel [155,156] and given by

$$\Delta P = 0.20\,\rho_f\ v_{drop}\ v_{sound}\ , \tag{15}$$

where v_{sound} is the speed of sound in liquid, may be used to predict the pressure at the liquid–solid interface.

5.2. Vapor layer thickness

When $T_w > T_{L,d}$, a thin vapor layer is formed beneath the drop following the impact as illustrated in Fig. 5. For a sessile drop with $T_w > T_L$, Biance et al. [157] proved experimentally that vapor layer thickness, δ, is strongly dependent on drop size,

$$\delta \sim \left[\frac{\rho_f\, k_f\, \mu_f (T_w - T_{sat})\ g}{h_{fg}\, \rho_v\, \sigma^2}\right]^{1/3} \left(\frac{d_{drop}}{2}\right)^{4/3}, \tag{16}$$

where subscript v refers to properties of the vapor film. Prat et al. [158] addressed the effects of surface roughness on vapor flow, noting that thickness of the vapor layer increases when the drop size increases relative to the scale of roughness. However, Celestini et al. [159] observed and predicted that vapor layer thickness increases for smaller drops, with $\delta \sim (d_{drop}/2)^{-3/2}$, which contradicts the dependence recommended by Biance et al. and given by Eq. (16).

Celestini and Kirstetter [127] found that an increase in voltage applied between the drop and the wall decreases vapor layer thickness. Ge and Fan [51,160] reported that vapor layer thickness decreases greatly with initial drop liquid subcooling.

Using computational methods, Chatzikyriakou et al. [161] showed that, for a sessile water drop, the vapor layer exhibits oscillatory behavior, but eventually settles to a thickness between 20 and 40 μm, which coincides well with the theoretical value of 28.9 μm obtained by Wachters et al. [162] for similar drop conditions. Inada et al. [163] measured vapor layer thickness for an impinging water drop and confirmed the oscillatory behavior of the vapor layer. During the recoil stage of the impact, they recorded a vapor layer thickness above 10 μm for a drop with 2 °C subcooling, and less than 5 μm with 88 °C subcooling.

Tran et al. [25] made direct measurements of vapor layer thickness of impinging water drops using light interferometry at different wavelengths as shown in Fig. 12(a). Fig. 12(b) shows the measured radial profile of film thickness. They noted that even for a low *We* of 3.5, vapor layer thickness is much smaller than that of a sessile Leidenfrost drop of about 20 μm. They also indicated that vapor layer thickness is close to the entrained air layer thickness measured indirectly by Thoroddsen et al. [164] for a drop

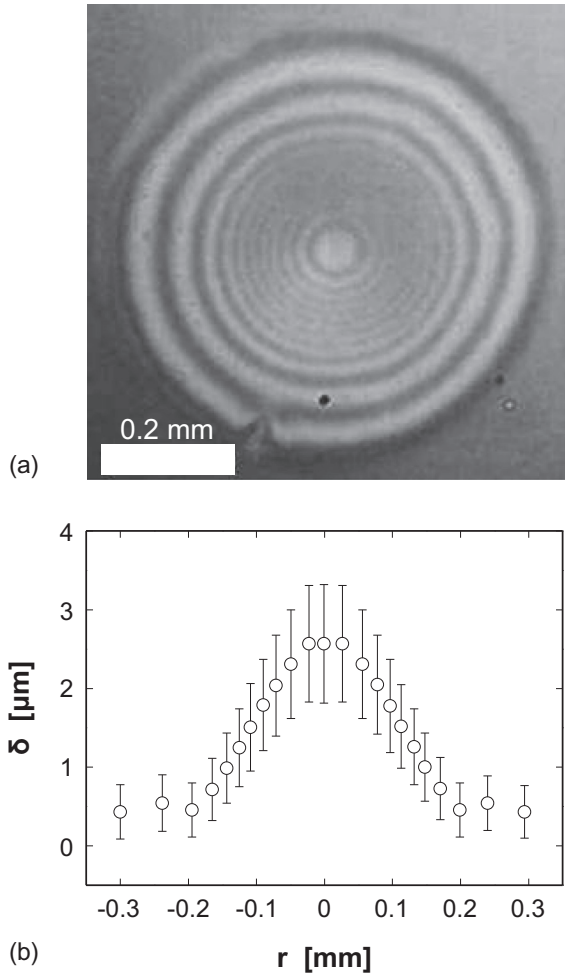

Fig. 12. Experimental measurements of vapor layer thickness of a water drop with *We* = 3.5 for T_w = 350 °C: (a) interference pattern showing thickness variations, and (b) radial profile of vapor layer thickness. Adapted from Tran et al. [25].

impacting an unheated wall. Later, Tran et al. [149] proposed scaling relations for vapor film thickness, δ, and velocity of vapor, v_v, out of the layer between the drop and the wall. They expressed dimensionless film thickness and velocity ($\delta^* = \delta/d_{drop}$ and $v^*_v = v_v/v_{drop}$) as

$$\delta^* \sim \beta^3 We^{-1/10}, \tag{17a}$$

and

$$v^*_v \sim \left[\frac{\rho_f k_g (T_w - T_{sat})}{\rho_g \mu_g h_{fg}}\right]^{1/2}, \tag{17b}$$

where β is a coefficient that depends on drop size. However, these scaling relations warrant further validation against experimental data.

5.3. Drop disintegration

In general, the critical Weber number, We_c, required for a water drop to break up upon impact on a heated wall in the film boiling regime is significantly lower ($50 < We_c < 80$) than reported for impact on an unheated dry wall ($200 < We_c < 260$) or on an unheated wall covered with a thin liquid film ($200 < We_c < 260$) [165]. Wachters and Westerling [14] observed three types of impact patterns for a water drop on a heated gold wall above 400 °C. They reported the drop disintegrates during the initial impact for $We > 80$, disintegrates after it begins to rise from the wall for $30 < We < 80$, and does not disintegrate for $We < 30$. Wang et al. [20] conducted experiments with 2.3-mm water drops at T_{sat} impacting a polished heated gold wall at $T_w = 400$ °C, and obtained a lower We range of $We < 23$ for the impact pattern with no drop disintegration.

Hatta et al. [166] proposed that critical Weber number for disintegration is influenced by several factors including liquid type, wall material, and wall superheat. For $T_w = 500$ °C, they measured We_c of about 50, 45 and 40 for Inconel 625, stainless steel, and silicon walls, respectively, in order of decreasing thermal conductivity. Ueda et al. [167] proposed $We_c = 65$ for water drops, and 75 for R113 drops on a copper wall at $T_w = 300$ °C. For water drops impacting a polished stainless steel wall with $260 < T_w < 400$ °C, Akhtar et al. [90] suggested five different impact patterns: pure rebound for $We \leqslant 15 \pm 5$, rebound with breakup for $20 \pm 5 < We < 50 \pm 5$, breakup limit for $We = We_c = 60 \pm 10$, typical splashing for $60 \pm 10 < We < 350 \pm 20$, and prompt splashing for $We > 350$. Chiu and Lin [168] observed three impact outcomes for a diesel drop impinging a polished stainless steel wall at $T_w = 450$ °C: regular reflection (rebound without breakup) for $We \leqslant 15$, breakup with one secondary droplet for $14 \leqslant We \leqslant 25$, and breakup with more than one secondary droplet for $We \geqslant 25$. They also provided a criterion for secondary droplet formation for a water-diesel compound drop.

Biance et al. [169] studied drop breakup due to rupture of the expanding/spreading lamella during the impact, triggered by a defect on the heated wall. The lamella rupture was shown to take place above a critical impact velocity, v_c, the magnitude of which decreases with increasing defect size, m, independent of drop size,

$$v_c \approx 1.4\sqrt{\frac{2\ \sigma}{\rho_f m}}. \tag{18}$$

Biance et al. also proposed the following relation for critical ratio of drop diameter to defect size corresponding to hole formation without splashing:

$$\frac{d_{drop}}{m} \approx 80. \tag{19}$$

There have also been studies addressing drop breakup during inclined impact. Yao and Cai [144] investigated the influence of impact angle on water drop breakup during impact with brass and chromium walls at $T_w = 400$ °C. As shown in Fig. 13, they proved that We_c increases with increasing impact angle, ϕ, since the drop is stabilized for large angle impact, and recommended the following correlation for We_c,

$$We_c = 12.89 + 0.85\,\phi - 0.0053\,\phi^2\,. \tag{20}$$

This trend relative to impact angle is consistent with experimental results by Chatzikyriakou et al. [170,171]. Karl and Frohn [148] pointed out the existence of a minimum impact angle, ϕ_{min}, below which no breakup would take place, and attributed this minimum to energy dissipation at the wall during the impact process. They explained that an increase in impact angle increases the tangential component of velocity, causing the drop to travel a greater distance to contact the wall, and therefore incurs a greater momentum loss. As shown in Fig. 14, they correlated the minimum impact angle according to

$$\phi_{min} = 45.7\left(\frac{R_z}{d_{drop}}\right)^{0.272}, \tag{21}$$

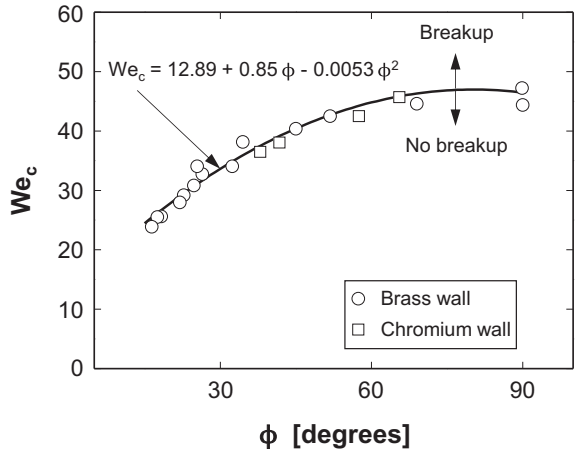

Fig. 13. Variation of critical Weber number, corresponding to water drop breakup upon impact with brass and chromium walls at 400 °C, with impact angle. Adapted from Yao and Cai [144].

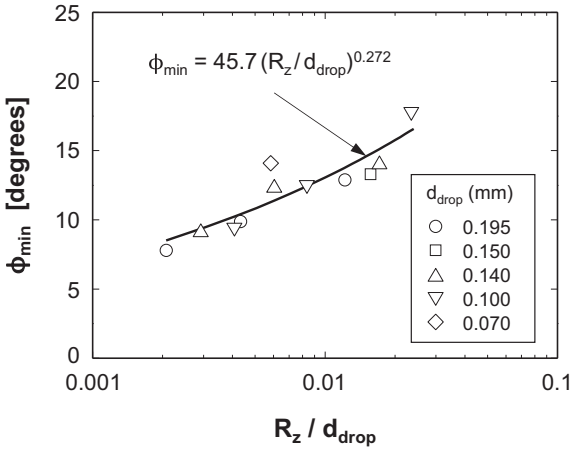

Fig. 14. Variation of minimum impact angle for disintegration of ethanol drop on chromium plated copper and steel at 325 °C with ratio of roughness depth to drop diameter. Adapted from Karl and Frohn [148].

for $0.002 < R_z/d_{drop} < 0.015$, where R_z is the height of surface roughness features. Karl and Frohn also reported that We_c is smaller for water than for ethanol, concluding that onset of drop breakup should not be based on We_c alone. They proposed an alternative empirical relation for onset of breakup for inclined impact based on $WeRe^{0.8}$, using normal component of impact velocity, $v_{drop,n}$, instead of We_c, where Re is the drop Reynolds number defined as

$$Re = \frac{\rho_f \, v_{drop} \, d_{drop}}{\mu_f}. \tag{22}$$

Kang and Lee [172] reported that a drop impacting a heated wall at $\phi = 30°$ does not break up, and tends to recover its original spherical shape during rebound because of low impact momentum normal to the wall. According to Chen et al. [173], a diesel drop with $v_{drop} < 1.5$ m/s and $0.5 < d_{drop} < 0.95$ mm incurs breakup when normal We is greater than 14, a value quite different from those recommended by Wachters and Westerling [14] and Wang et al. [20]. Chen et al. suggested that breakup is influenced by several factors such as T_w and liquid subcooling, which influence liquid properties.

5.4. Drop rebound

5.4.1. Rebound mechanism

Fig. 15, which was obtained by the present authors, shows how a low velocity drop impacting a heated wall at $T_w > T_{L,d}$ will spread laterally, then recoil and bounce off the heated wall. Following the events depicted in Fig. 15, the drop will fall by gravity onto the heated wall and will repeat the same process several times. Absent any secondary droplet formation, this rebound behavior is also termed *non-wetting interaction* or *reflection*. It should be emphasized that the rebound behavior shown in Fig. 15 is qualitatively similar to, but fundamentally quite different from rebound on unheated or pre-wetted walls. For unheated hydrophobic or super-hydrophobic walls, rebound is governed by liquid–solid contact angle [174,175]. While, for rebound on a pre-wetted wall, the drop and liquid are separated by a thin air layer, and We_c for rebound spans a range of values instead of occurring at a specific value [176,177]. For rebound on a heated wall, as shown in Fig. 15, the rebound at high T_w is influenced by pressure from the vapor layer as discussed earlier. Richter et al. [178] indicated that this rebound is different from the thermal rebound achieved at low T_w. They described the rebound at low T_w as drop breakup into secondary droplets that levitate completely above the wall, merging again into a single upward-moving new drop.

Deng and Gomez [52] found that electrically charged liquid drops prevent rebound on a heated wall. Celestini et al. [159] observed an unexpected behavior of Leidenfrost drops during the later stage of evaporation, where drop size decreases to a value below lubrication limit, and the drop rebounds from the heated wall spontaneously. Anders et al. [106] found that loss of velocity in rebound is a function of We based on normal component of impact velocity, $v_{drop,n}$. Interestingly, Antonini et al. [179] observed drop rebound on a variety of wall types and temperatures, including superhydrophobic wall, hot wall, and even dry ice, with wall temperatures ranging from 300 °C down to below −79 °C. However, they reported rebound mechanisms on the different walls are substantially different.

Biance et al. [180] used analogy with spring bouncing against a wall to explain the drop rebound process, Fig. 16, and explained the rebound by drop elasticity. They identified two different regimes of drop bouncing based on magnitude of We. In the first regime, which is encountered at high We, drop impact inertia is much larger than surface tension, rendering the rebound less elastic. This regime is associated with energy loss due to dissipation during the spread, and partitioning of energy between drop oscillation and spread at rebound. With increasing impact velocity, the portion of energy consumed by oscillation increases, which is why this regime lacks elasticity. Elasticity is also reduced when drop diameter exceeds capillary length, $(\sigma/(\rho_f g))^{1/2}$, causing the drop to oscillate without bouncing, regardless of impact velocity. The second drop bouncing regime identified by Biance et al. is the quasi-elastic regime corresponds to low We (typically $We \ll 1$), where the drop may bounce hundreds of times, always coming back to the same height. In this regime, rebound is closely associated with drop oscillation, and the bouncing drop maximizes elasticity by adjusting its flight time to oscillation time. Then, successive bouncing of the drop reaches resonant state where energy loss is minimized.

5.4.2. Numerical approaches

In numerical studies of drop rebound, two main approaches have been used: with and without a vapor layer model. The latter neglects the vapor flow by using free slip condition at the liquid–solid contact surface and a contact angle of 180° (*i.e.*, assuming non-wetting contact) [181,182]. With the approach including effects of the vapor layer beneath the liquid drop, the vapor flow is solved separately to determine the vapor's pressure and velocity distributions [51,160,183–186]. In this second approach, heat transfer is accounted for within each phase as well as across the solid–vapor and liquid–vapor interfaces. Fujimoto and Hatta

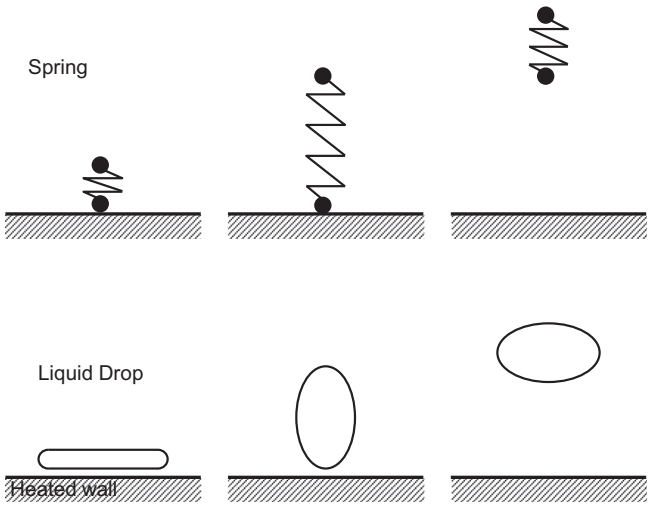

Fig. 16. Spring model of drop rebound. Adapted from Biance et al. [180].

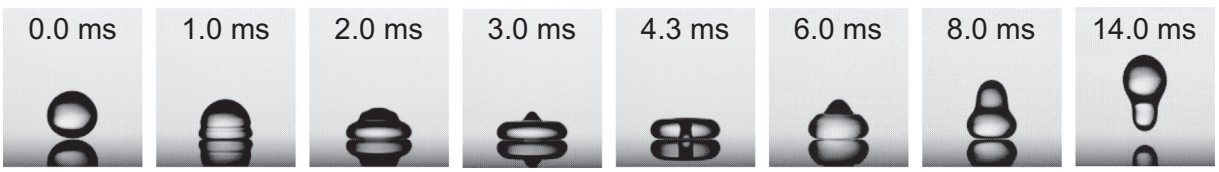

Fig. 15. Butanol drop rebound from a heated wall for $T_w = 384$ °C and $We = 4$.

[187] suggested the non-slip condition can be used in simulating the rebound before the spread achieves maximum extent, but the bottom boundary condition for the drop should be switched from non-slip to free-slip at the moment the spread is terminated. They also showed that the drop's geometrical parameters (diameter and height) are similar for heated and unheated walls during the spread, but not during the recoil. Chizhov and Takayama [188] developed a model for the vapor layer based on simplified compressible Navier–Stokes equations.

5.4.3. Residence time

Residence time of the drop, t_r, is defined as the duration from first contact with, to first bounce from the wall. Wachters and Westerling [14], Tran et al. [149], Ge and Fan [160], Ueda et al. [167], and Makino and Michiyoshi [189] all reported that t_r is strongly dependent on drop size, and can be approximated by the period of a freely oscillating drop, which is given by [190]

$$t_o = \frac{\pi}{4}\sqrt{\frac{\rho_f d_{drop}^3}{\sigma}} \quad . \tag{23}$$

Richard et al. [191] obtained residence time data for non–heated walls that agree with Eq. (23). Tran et al. suggested that t_r is insensitive to wall temperature, impact velocity, or surface finish. Akao et al. [192] determined that Eq. (23) does not hold well against their experimental data. Chandra and Avedisian [19] noted that their measured residence times are larger than predicted by Eq. (23). And Chatzikyriakou et al. [170] found that Eq. (23) underestimates residue time for a small impact angle of $\phi = 5°$. Several other studies [166,173,180] also indicated that the coefficient $\pi/4$ in Eq. (23) does not agree well with experimental data. To improve agreement with the data, they recommended the more general form

$$t_r = C\sqrt{\frac{\rho_f d_{drop}^3}{\sigma}}, \tag{24}$$

along with correlations for non-dimensional residence time, τ_r, according to the relation

$$\tau_r = \frac{v_{drop}\, t_r}{d_{drop}} = C\ We^n \quad . \tag{25}$$

Table 1 provides a summary of correlations for t_r or τ_r by different investigators.

For rebound on a hydrophobic heated wall, Park et al. [84] measured a residence time of drop-solid direct contact on the order of 1 ms for $110 < T_w < 210$ °C (*i.e.,* below $T_{L,d}$) independent of T_w, which is similar to residence time in the film boiling regime. However, their time-domain thermo-reflectance measurements showed that residence time decreases to a minimum of 0.025 ms with increasing T_w because of the vapor trapped beneath. In a recent study, Negeed et al. [194] suggested that residence time depends mostly on *We* and contact angle.

5.4.4. Spreading scale

Drop spread is more commonly examined in studies of drop impact on a solid dry wall, mainly for the purpose of describing wetting or cooling effects [195,196]. When $T_w > T_{L,d}$, a vapor layer is generated between the drop and heated wall, preventing the drop from wetting the wall [101]. Spreading scale is defined as diameter D of the flattened area [19] as depicted in Fig. 5.

Manzello and Yang [197] showed that drop spreading scale in the film boiling regime is larger than in the film evaporation and nucleate boiling regimes. Hatta et al. [166] found no significant influence of *Re* on *spreading factor* $D^* = D/d_{drop}$, which they explained by negligible viscous dissipation in the absence of direct drop contact with the wall [180,191]. For an unheated wall, drop spread is affected greatly by contact angle and surface roughness. However, for heated walls with $T_{L,d} > T_w$, drop spread is far less dependent on surface roughness in the presence of a vapor layer between the drop and the wall. In their simulations of drop deformation in the absence of heat transfer, Karl et al. [181] showed that general deformation behavior is independent of liquid properties, drop diameter, or impact velocity, but, maximum drop deformation is influenced by drop velocity and liquid type. Bertola [198] suggested that adding a small amount of polymer in Newtonian liquids can decrease spreading scale.

Negeed et al. [199] investigated the influence of coating the heated wall with oxide layer (4.5–12.6 μm) on drop impact. They found that increasing oxide layer thickness decreases maximum spreading scale, but reported similar drop impact behavior for surfaces with versus without oxide layer oxide [200]: maximum spreading scale increases with increasing *We*, drop size, or impact velocity, or decreasing wall temperature. Negeed et al. [201] explored the effects of both oxide layer thickness and surface roughness (R_a = 0.04–10 μm), and found that a ratio of roughness to oxide layer thickness between 0.01 and 1.0 increases maximum spreading factor, D^*_{max}, while a ratio between 1.0 and 2.5 has the opposite effect. In their more recent work [194,202], they found that applying a TiO_2 superhydrophilic coating on the heated wall greatly increases wettability, leading to larger D^*_{max}. Castanet et al. [203] suggested that liquid motion inside the drop is accelerated radially by the vapor flow, which greatly increases spreading scale for low viscosity liquids according to $D^*_{max} \sim We^{1/2}$. For high viscosity liquids, this dependence was modified by incorporating viscosity effects according to $D^*_{max} \sim Re^{1/5}We^{1/2}$.

Tran et al. [25] correlated maximum spreading factor according to $D^*_{max} \sim We^{2/5}$, in which Weber number dependence is stronger than for a super-hydrophobic surface, where $D^*_{max} \sim We^{1/4}$ [204,205]. Tran et al. attributed this difference to evaporating vapor shooting radially outwards and shearing the liquid along.

Table 1
Summary of correlations for drop residence time.

Authors	Fluid(s)	Wall material(s)	Test conditions	Correlations
Biance et al. [180]	Water	Steel	d_{drop} = 0–4 mm v_{drop} = 0–1.5 m/s	$t_r = 0.937\sqrt{\frac{\rho_f d_{drop}^3}{\sigma}}$
Chen et al. [173]	Diesel oil	Polished stainless steel	d_{drop} = 0.5–0.95 mm v_{drop} = 0.93–1.767 m/s ϕ = 20–60°	$t_r = 1.12\sqrt{\frac{\rho_f d_{drop}^3}{\sigma}}$
Hatta et al. [166]	Water	Inconel alloy 625, stainless steel, silicon	d_{drop} = 0.3–0.6 mm *We* = 10–65	$\tau_r = 1.25\,We^{0.37}$
Chen et al. [193]	Water drop enclosed in diesel oil layer	Polished stainless steel	d_{drop} = 0.74–0.97 mm v_{drop} = 0.5–1.18 m/s ϕ = 20–60°	$\tau_r = 1.12\,We^{1/2}$
Liang et al. [32]	Water, ethanol and butanol	Polished stainless steel	d_{drop} = 1.56–2.06 mm v_{drop} = 0.24–2.13 m/s	$\tau_r = 1.032\,We^{0.494}$

In their follow-up work [149,152], they correlated maximum spreading factor for different structured surfaces according to $D^*_{max} \sim We^{3/10}$.

Table 2 provides a summary of maximum spreading factor correlations recommended by different investigators. It should be emphasized that *We* in this table is based on normal component of drop velocity.

5.5. Heat transfer

5.5.1. Models

Gottfried and Bell [209] developed an analytical model to predict heat transfer during film boiling, accounting for heat conduction across the vapor layer, thermal radiation from the heated wall, and molecular diffusion along the top surface of the drop. Inada and Yang [210] conducted theoretical analysis of film boiling heat transfer for saturated drops, and showed, for $12.3 < We < 50$, that Nusselt number can be predicted according to

$$Nu = 2.8We_v^{-0.56}(We/2+13)^{-0.56}Bo^{-0.056}\ Pr_f^{0.31}, \tag{26}$$

where We_v and *Bo* are Weber number of the vapor layer and Bond number, which are defined, respectively, as

$$We_v = \sqrt{\frac{\rho_g\, v_v^2 z_b^2}{\sigma\, d_{drop}}}, \tag{27a}$$

and

$$Bo = \frac{g(\rho_f - \rho_g)d_{drop}^2}{\sigma}, \tag{27b}$$

and z_b is the axial coordinate at the drop base.

It is well acknowledged that a strong decline in the heated wall temperature is incurred at the instant of drop impact. Wruck and Renz [211] estimated this initial decline at 10^5 °C/s. Shi et al. [212] measured the temperature drop and corresponding heat transfer rate using a high sensitivity, two-dimensional surface temperature probe made from 0.03-mm alumel-chromel film. Their results suggested that momentary liquid–solid contact does occur even when $T_w > T_{L,d}$. Therefore, they identified two drop impact cooling regimes: cooling with wetting contact and cooling without wetting contact. They also found that drop impact heat transfer is influenced mostly by initial wall temperature, as well as by impact velocity, drop diameter, impact angle, and liquid subcooling, and correlated the drop's heat transfer rate, *Q*, according to

$$Q = Q_n(\sin\phi)^{0.69}, \tag{28}$$

where Q_n is the heat transferred from the wall for normal impact.

Xie and Zhou [213] divided drop evaporation in film boiling into two stages: recoil and spherical evaporation, and proposed heat transfer models for each stage in terms of *We*, d_{drop}, wall superheat, and surface wettability, neglecting the effects of drop spread due to its short duration. They also recommended the following theoretically based correlation for drop evaporation lifetime, defined as the duration from first contact to complete evaporation of the drop,

Table 2
Summary of correlations for maximum spreading factor.

Authors	Fluid(s)	Wall material(s)	Test conditions	Correlations
Tran et al. [25]	FC-72, water	Polished silicon	d_{drop} = 1.1–2.2 mm *We* = 0.5–600	$D^*_{max} = C\,We^{2/5}$
Tran et al. [149]	Water	Silicon micro-structured surface	d_{drop} = 2.2 mm v_{drop} = 0.4–4 m/s	$D^*_{max} = C\,We^{3/10}$
Nair et al. [152]	FC-72	Silicon carbon-nanofiber surface	d_{drop} = 1.1 mm *We* = 10–1000	$D^*_{max} = C\,We^{3/10}$
Ng et al. [153]	Deionized water	Vibrating copper plate	d_{drop} ~ mm scale *We* = 60–200	$D^*_{max} = C\,We^{1/4}$
Ueda et al. [167]	Water, R113	Copper, stainless steel	d_{drop} = 0.9–3.0 mm v_{drop} = 0.6–3.0 m/s	$D^*_{max} = 0.87\left(\frac{We}{6}+2\right)^{1/2}$
Akao et al. [192]	Water, ethanol, acetic acid	Copper	d_{drop} = 2.1–2.9 mm v_{drop} = 0.66–3.21 m/s	$D^*_{max} = 0.631\,We^{0.39}$
Hatta et al. [166,206]	Water	Inconel 625, stainless steel, silicon	d_{drop} = 0.3–0.6 mm v_{drop} = 1.48–5.7 m/s	$D^*_{max} = 0.093\ \ We^{0.74} + 1$
Karl and Frohn [148]	Water, ethanol	Chromium-plated copper, Chromium-plated steel	d_{drop} = 0.07–0.26 mm *We* = 0–60	$D^{*3}_{max} - \left[\frac{We}{6}\frac{\{1+(1-0.263\ We^{0.257})^2\}}{2}+2\right]D^*_{max} + \frac{4}{3} = 0$
Chen et al. [173]	Diesel oil	Polished stainless steel	d_{drop} = 0.5–0.95 mm v_{drop} = 0.93–1.767 m/s ϕ = 20–60°	$D^{*3}_{max} - 2\ \ D^*_{max}(0.052\ \ We+1) + \frac{4}{3} = 0$
Chandra and Avedisian [19]	Heptane	Stainless steel	d_{drop} = 1.5 mm v_{drop} = 0.93 m/s	$D^*_{max} = \left(\frac{We}{3}+4\right)^{1/2}$
Biance et al. [180]	Water	Steel	d_{drop} = 0–4 mm v_{drop} = 0–1.5 m/s	$D^*_{max} = C\,We^{1/4}$
Chatzikyriakou et al. [161]	Water	–	d_{drop} = 0.89–1 mm *We* = 3–40	$D^*_{max} = C\,We^{0.23}$
Akhtar and Yule [207]	Water	Stainless steel	d_{drop} = 0.02–0.16 mm v_{drop} = 5–18 m/s	$D^*_{max} = 0.0065\,We + 3.61$
Antonini et al. [179]	Water	Polished aluminum, silicon wafer	d_{drop} = 2.2 mm *We* = 1–100	$D^*_{max} = C\,We^{1/4}$
Lastakowski et al. [208]	Ethanol, isopropanol-glycerol mixtures	Smooth silicon wafer	d_{drop} = 1.6–3.6 mm v_{drop} = 1–4 m/s	$D^*_{max} = C\,We^{1/4}$
Castanet et al. [203]	Water, ethanol, water-glycol mixtures	Nickel	d_{drop} = 0.1–0.3 mm	$D^*_{max} = 0.077\,Re^{1/5}\,We^{1/2} + 1$ for high viscosity liquids
			v_{drop} = 0.84–7.7 m/s	$D^*_{max} = 0.23\ \ We^{1/2} + 1$ for low viscosity liquids
Liang et al. [32]	Water, ethanol and butanol	Polished stainless steel	d_{drop} = 1.56–2.06 mm v_{drop} = 0.24–2.13 m/s	$D^*_{max} = 0.788\ \ We^{0.306}$

$$t_c = \frac{3.76\left[(d_{drop}/2)^{2.25} - \frac{9}{16}\ C\ \frac{(D_{max}/2)A_2^{0.25}}{A_1^{0.25}}\right]^{5/9}}{A_1^{0.75}A_2^{0.25}} + \frac{C\,d_{drop}^2}{A_1}, \tag{29a}$$

where

$$A_1 = \frac{k_v(T_w - T_{sat})}{\rho_f\ h_{fg}}, \tag{29b}$$

$$A_2 = \frac{\rho_v g}{\mu_v}, \tag{29c}$$

and $C \approx 0.0024$.

Ge and Fan [51] found numerically that impact of a heptane drop yields much smaller decline in wall temperature compared to a water drop. They also showed how wall temperature declines mainly during the drop spreading stage, and recovers during the recoil, due to presence of a fully established vapor layer. During the spread, heat flux is relatively uniform through the liquid–solid contact area except near the drop's outer periphery, and is relatively small during the recoil. Additionally, the vapor layer thickness and wall heat flux are closely related to initial subcooling of the drop. Chatzikyriakou et al. [214] measured heat transfer between the heated wall and a non-wetting water drop in the film boiling regime using transient high resolution infrared microscopy. Their measurements revealed the total heat transferred by a 1.5-mm drop is 0.19 J, with peak heat flux of 3.5 MW/m^2 and peak transient wall temperature decrease of 47 °C occurring during the first 10 ms following impact. They also reported that the wall temperature drop and heat flux distribution are highly non-uniform for inclined impact.

Using a two-color laser-induced fluorescence (LIF) technique [215], Castanet et al. [27] measured both temporal and spatial distributions of drop temperature. They showed that the change in drop temperature during impact in the film boiling regime depends on normal impact velocity but not on wall temperature. They measured up to 40 °C increase in drop temperature in the case of splashing, but far less in the case of rebound. Later, Dunand et al. [216,217] estimated the loss of drop mass due to vaporization by comparing heat removal from the wall, using a semi-analytical inverse heat conduction model, to sensible heat gain by the drop, using the LIF technique. They determined that the main contributor to wall cooling is the drop's sensible heat rise for large drops, and drop evaporation for small drops. For drops within an air stream, Buckingham and Haji-Sheikh [218], and Thomas et al. [219] identified two heat transfer regions: radiation-dominated and convection-dominated.

5.5.2. Impact velocity effects

Pedersen [142] showed that increasing impact velocity enhances drop heat transfer in the non-wetting regime, but wall temperature has only a secondary effect. Simulations by Pournaderi and Pishevar [220] confirmed the enhancement effect of impact velocity. On the other hand, Labeish [221] found that increasing impact velocity for water drops from 2.0 to 6.2 m/s decreases heat removal rate by 30%, and the effect of impact velocity is comparatively small for alcohol drops. Akhtar and Nasr [165] shed further light on this effect by verifying experimentally that increasing impact velocity does not always enhance heat transfer, especially in the film boiling regime. Instead, they suggested the existence of an optimum drop velocity value beyond which heat transfer deteriorates for a given drop size. Gradeck et al. [222] estimated the heat transfer coefficient of the drop in the film boiling regime by measuring the rate of heat released from the wall. Their results demonstrated weak dependence of the heat transfer coefficient on *We*.

Overall, there is no consensus among investigators regarding the influence of impact velocity on drop heat transfer, and more experimental measurements and modeling are needed to clarify this influence.

5.5.3. Drop size effects

Most studies suggested that drop lifetime decreases gradually with increasing T_w when $T_w > T_{L,d}$. However, Xiong and Yuen [80] suggested that lifetime of a small drop tends to decrease only slowly or not at all with increasing T_w. They explained this trend by induced air motion above the hot wall, which tends to push the drop away from the wall, increasing lifetime for smaller drops in contrast with larger drops. Xiong and Yuen also showed that heat transfer rate for pure drops and mixed hydrocarbon fuels is maximum for a drop diameter of about 0.5 mm.

Labeish [221] observed a slight decrease in heat removal rate in film boiling with increasing drop size. Labeish and Pimenov [223] noted that contact of a water drop with the wall lasts only about 2.5 ms in the film boiling regime. Choi and Hong [224] investigated the influence of drop size on film boiling heat transfer for a heated disc that was rotated about its axis. At a relatively low rotational speed of 600 rpm, they observed impact phenomena similar to those on a stationary wall, with larger drops providing better heat transfer than smaller drops. On the other hand, results for speeds exceeding 1200 rpm pointed to a reversal in the dependence of heat transfer on drop size, which was attributed by Choi and Hong to interactions with the surrounding air boundary layer.

5.5.4. Influences of other parameters

Qiao and Chandra [97] performed drop impact experiments in low gravity and pointed to difficulty maintaining film boiling as pressure by vapor beneath the drop pushes the drop away from the wall, which greatly decreases heat transfer between the heated wall and the drop. Emmerson [114] found that maximum evaporation time of a sessile water drop decreases with increasing T_L at any given pressure, regardless of thermal diffusivity of the heated wall. Chandra and Aziz [225] experimentally investigated the influence of surface roughness on drop evaporation, and suggested two different regimes depending on surface roughness feature size compared to thickness of the vapor layer of 25–50 μm. They found that, when surface roughness is much smaller than vapor layer thickness, small increases in surface roughness do not affect drop evaporation. But when surface roughness feature size approaches the vapor layer thickness, increasing roughness size decreases drop lifetime because of bubble formation within the drop. Fatehi and Kaviany [226] suggested that depositing a relatively thick porous layer on the heated wall greatly benefits drop evaporation. Pournaderi and Pishevar [220] noted that adding polymer in water drops has no significant influence on drop evaporation, while use of surfactant enhances heat transfer by increasing residence time and maintaining better drop contact with the wall.

5.6. Secondary atomization

5.6.1. Single drop impact

Cossali et al. [94] reported that production of secondary droplets commences immediately following impact in the film boiling regime, compared to a few milliseconds later in nucleate boiling. There are also substantial differences in the directions of emitted secondary droplets between the two regimes. As shown earlier in Fig. 9 for nucleate boiling, a larger number of small secondary droplets are ejected normal to the heated wall, whereas, larger and fewer secondary droplets are ejected in radial orientations immediately following impact in film boiling, as shown in Fig. 17. Cossali et al. attributed the larger size of secondary droplets in film boiling to breakup of the spreading liquid

film. Additionally, an increase in liquid viscosity considerably increases the size of secondary droplets in the film boiling regime, but has no significant effect in nucleate boiling. Follow-up work by Cossali et al. [95] revealed that, in contrast to the minor effects of surface roughness on secondary droplet size in nucleate boiling, an order of magnitude decrease in surface roughness in film boiling decreases average size of secondary droplets by more than 15%. Additionally, increasing impact velocity in film boiling increases lamella spread, which decreases the size of secondary droplets. Moita and Moreira [98] also examined surface roughness effects and drew conclusions similar to those of Cossali et al.

Akhtar and Yule [207] obtained the following correlations for secondary droplets number, N, and average ejection angle, α, with the heated wall for $100 < We < 750$ and $260 < T_w < 400$ °C:

$$N = 0.0427\,We + 10.46 \quad , \tag{30a}$$

and

$$\alpha = 85.99\ e^{-0.0045\ We} \quad , \tag{30b}$$

respectively. They also proposed the following correlation for Sauter Mean Diameter, d_{32}, of secondary droplets for $We > 200$:

$$\frac{d_{32}}{d_{drop}} = C + \left(\frac{60}{We}\right)^{n}, \quad 1 < n < 1.5. \tag{31}$$

To better match their data for $We > 200$, Moita and Moreira [98] recommended broadening the range of exponent n in Eq. (31) to $0.1 < n < 2.5$, but, in a separate study [99], they adopted a relation originally devised for non–heated walls to correlate their own heated wall data,

$$\frac{d_{32}}{d_{drop}} = C\,We^{-0.6}Re^{-0.23} \quad . \tag{32}$$

They also reported that, in the film-boiling regime, secondary droplets are formed by radial disruption of the drop's rim shortly following impact, as well as from rupture of bridges surrounding Rayleigh-Bénard cells in the spreading film, which were clearly captured by Chaves et al. [96]. The images in Fig. 18(a) show convection cells in the liquid film surrounded by thin liquid bridges. When the spreading liquid film reaches a certain thickness, the liquid bridges break up, leaving tiny bridge droplets behind as illustrated schematically in Fig. 18(b).

Experiments by Moreira et al. [227] showed that the size of secondary droplets is weakly dependent on impact angle for large impact angles ($\phi > 45°$), but becomes considerably smaller for small impact angles ($\phi < 15°$). They reported that the effect of impact angle is less significant for isooctane compared to that for water, which suggests that the influence of impact angle becomes stronger with increasing surface tension.

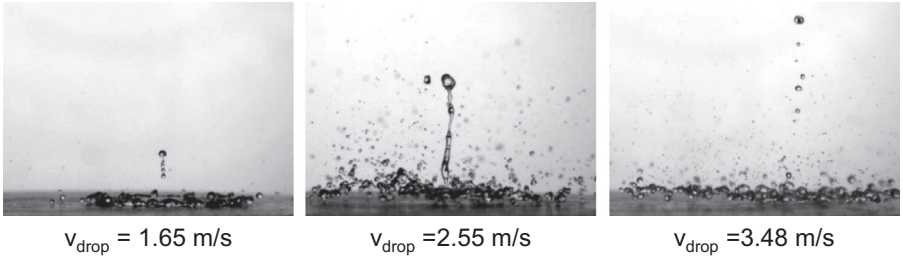

Fig. 17. Secondary droplet atomization in film boiling of a water drop for $T_w = 260$ °C and $\tau = 2$. Adapted from Cossali et al. [94].

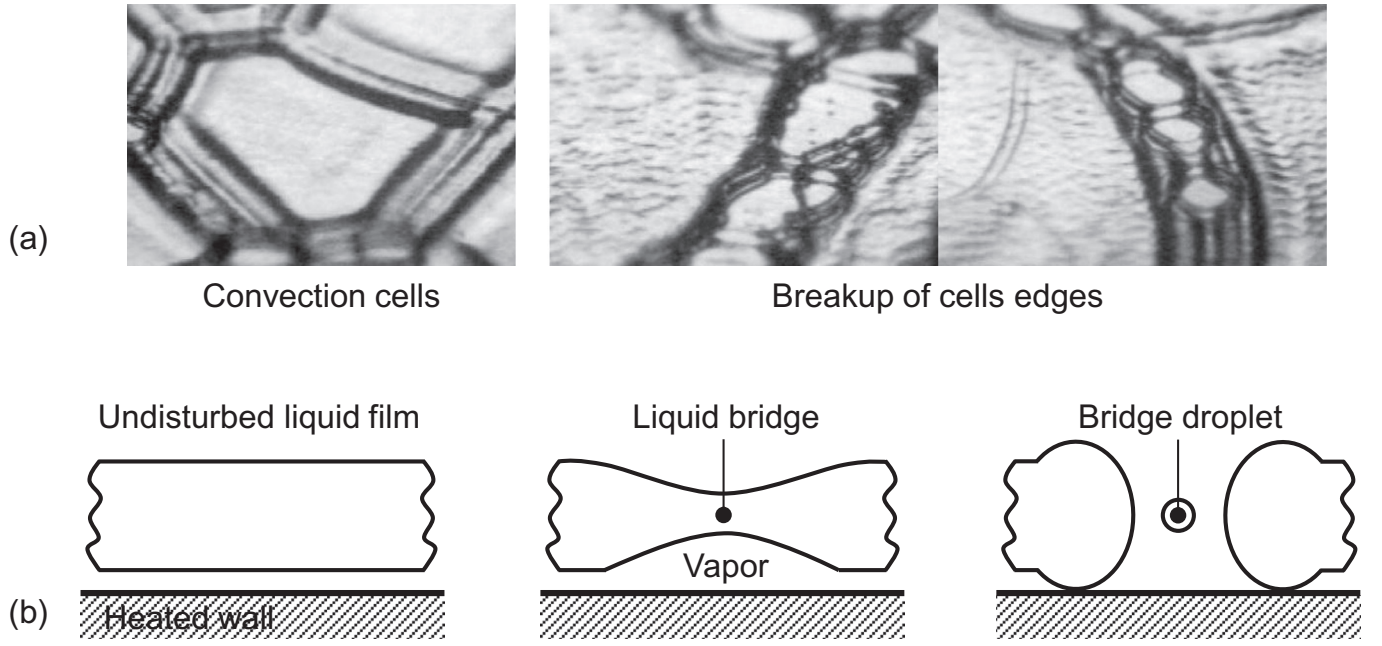

Fig. 18. Breakup of bridges surrounding Rayleigh-Bénard cells is spreading liquid film for $We = 300$ and $T_w = 200$ °C. (a) Images of cells and bridge breakup. (b) Schematic representation of bridge breakup and bridge droplet formation. Adapted from Chaves et al. [96].

An interesting phenomenon was observed by Cossali et al. [94,95] during water drop impact for $T_w > 230$ °C. As shown in Fig. 17, a liquid jet is ejected vertically upwards from the center of the impacting drop. They reported this jet behavior is governed by wall temperature and impact velocity and, to a lesser extent, by surface roughness, and proposed that the jet is the outcome of a pressure wave at the impact point caused by rapid formation of a central vapor bubble, but this hypothesis has not been verified experimentally. However, Tran et al. [149] observed the central jet only on structured surfaces and could not reproduce it on a smooth surface, and suggested the jet is caused by liquid converging toward the axis of the flattened drop. Recently, Liang et al. [32] observed the central jet for NaCl solution, but not for water, ethanol or butanol. They suggested that the key reason behind differences with the findings of Cossali et al. [94,95] is surface roughness. Using experimental evidence, Liang et al. attributed the jet formation to initial air entrainment and violent nucleation. To date, the mechanism of central jet formation remains an open question worthy of further investigation.

5.6.2. Multi-drop impact

For multi-drop impact during film boiling, Cossali et al. [228] indicated that the ratio of number of secondary droplets produced by the impact divided by number of impacting drops is substantially smaller than for single drop impact, and explained this reduction by liquid removal from the wall resulting from interaction between the impacting drops. Later, Cossali et al. [229] investigated the effect of horizontal spacing between adjacent drops, and showed that a larger spacing results in smaller secondary droplets at the beginning of interaction between the drops, but the trend is reversed at a later time.

Minamikawa et al. [230] numerically studied successive impact of two drops on a heated wall. In the film boiling regime, they predicted formation of a distorted crown following the impact, the size of which is strongly dependent on vertical spacing between the drops. Fujimoto et al. [231] observed the crown formation experimentally only for low *We* during film boiling with successive drop impact. Richter et al. [232] found that the size of secondary droplets for successive impact increases with decreasing drop spacing. And, in another study [140], they showed that the size of secondary droplets decreases with increasing *We*. They pointed out that, by reducing vertical spacing between the drops to enhance intensity of drop interaction, secondary droplets become concentrated near the heated wall, instead of being ejected away from the wall, and the velocity of secondary droplets increases.

Despite important contributions by several investigators to the understanding of multi-drop impact, both laterally and vertically, this topic remains quite elusive, and warrants further comprehensive study, given its importance as a building block to understanding drop behavior in many spray cooling applications.

6. Concluding remarks

This article reviewed published literatures addressing fluid mechanics and heat transfer mechanisms of liquid drop impact on a heated wall. The review is divided into four parts, each centered on one of the main heat transfer regimes of film evaporation, nucleate boiling, transition boiling, and film boiling. Key observations from this review can be summarized as follows.

(1) The topics of drop impact and ensuing heat transfer have benefitted greatly from recent use of diagnostics methods such as total internal reflection and interferometric high-speed imaging. Further advances in diagnostics methods are expected to provide more detailed insights into some of the more elusive aspects of the impact process, especially the interface between the drop and the heated wall, which will undoubtedly contribute to development of more accurate drop heat transfer models.

(2) For the film evaporation regime, more comprehensive heat transfer models are needed that would account for not only conduction across the liquid film but also internal motion and convection within the drop, and effects of gas flow induced around the drop. Additionally, better understanding of impact behavior, from the onset of impingement and during subsequent oscillations leading to equilibrium state, is required to improve heat transfer models. There is also a need to improve understanding of the different stages of film evaporation and critical receding contact angle for fluids other than water.

(3) There is lack of understanding of mechanisms governing critical heat flux (CHF), which constitutes the upper limit for the nucleate boiling regime, evidenced by inconsistent findings among different investigators. The significance of CHF to many applications warrants further systematic experimental and modeling work.

(4) The transition boiling regime, which extends between the CHF and Leidenfrost points, has received very limited attention in prior studies, and developing predictive models or correlations for this regime will require carefully designed experiments and better diagnostics.

(5) The Leidenfrost temperature is very important to drop impact on a heated wall, setting the boundary between very slow cooling during film boiling and faster cooling during transition boiling. While this temperature has been the focus of many studies, no reliable correlations or models are presently available for this parameter. Therefore, experiments are needed to investigate all possible influences on vapor layer development beneath the drop, including drop size and momentum, and wall material and surface roughness, for many liquids with vastly different thermophysical properties.

(6) Film boiling has received significant attention in past studies, with two limiting regimes clearly identified: rebound and breakup. A number of models have been developed for the rebound regime using different boundary conditions along the interface between the liquid drop and the vapor flow beneath. Also available are correlations to predict the threshold for drop breakup following impact. Future improvements in understanding heat transfer in the film boiling regime will rely heavily on accurate modeling of the vapor layer and better models for secondary droplet atomization.

Acknowledgements

Support of the National Natural Science Foundation of China under Grant No. 51506023, and the China Postdoctoral Science Foundation under Grant No. 2016T90220 is gratefully acknowledged.

References

[1] L.V. Zhang, J. Toole, K. Fezzaa, R.D. Deegan, Evolution of the ejecta sheet from the impact of a drop with a deep pool, J. Fluid Mech. 690 (2012) 5–15.
[2] M.J. Thoraval, K. Takehara, T.G. Etoh, S.T. Thoroddsen, Drop impact entrapment of bubble rings, J. Fluid Mech. 724 (2013) 234–258.
[3] S.T. Thoroddsen, T.G. Etoh, K. Takehara, High-speed imaging of drops and bubbles, Ann. Rev. Fluid Mech. 40 (2008) 257–285.
[4] A. Prosperetti, H.N. Oguz, The impact of drops on liquid surfaces and the underwater noise of rain, Ann. Rev. Fluid Mech. 25 (1993) 577–602.
[5] M. Rein, Phenomena of liquid drop impact on solid and liquid surfaces, Fluid Dyn. Res. 12 (1993) 61–93.
[6] A.L. Yarin, Drop impact dynamics: splashing, spreading, receding, bouncing. . ., Ann. Rev. Fluid Mech. 38 (2006) 159–192.

[7] M. Marengo, C. Antonini, I.V. Roisman, C. Tropea, Drop collisions with simple and complex surfaces, Curr. Opin. Colloid Interface Sci. 16 (2011) 292–302.
[8] A.L.N. Moreira, A.S. Moita, M.R. Panao, Advances and challenges in explaining fuel spray impingement: how much of single droplet impact research is useful?, Prog Energy Combust. Sci. 36 (2010) 554–580.
[9] C. Josserand, S.T. Thoroddsen, Drop impact on solid surface, Ann. Rev. Fluid Mech. 48 (2016) 365–391.
[10] M.R.O. Panão, A.L.N. Moreira, Flow characteristics of spray impingement in PFI injection systems, Exp. Fluids 39 (2005) 364–374.
[11] S. Shen, G. Liang, Y. Guo, R. Liu, X. Mu, Heat transfer performance and bundle-depth effect in horizontal-tube falling film evaporators, Desalin. Water Treat. 51 (2013) 830–836.
[12] M. Pasandideh-Fard, S.D. Aziz, S. Chandra, J. Mostaghimi, Cooling effectiveness of a water drop impinging on a hot surface, Int. J. Heat Fluid Flow 22 (2001) 201–210.
[13] M. Visaria, I. Mudawar, Application of two-phase spray cooling for thermal management of electronic devices, IEEE Trans. Compon. Packag. Technol. 32 (2009) 784–793.
[14] L.H.J. Wachters, N.A.J. Westerling, The heat transfer from a hot wall to impinging water drops in the spheroidal state, Chem. Eng. Sci. 21 (1966) 1047–1056.
[15] R. Bhardwaj, J.P. Longtin, D. Attinger, Interfacial temperature measurements, high-speed visualization and finite-element simulations of droplet impact and evaporation on a solid surface, Int. J. Heat Mass Transfer 53 (2010) 3733–3744.
[16] Z. Pan, H. Wang, Symmetry-to-asymmetry transition of Marangoni flow at a convex volatizing meniscus, Microfluid. Nanofluid. 9 (2010) 657–669.
[17] Y.S. Ko, S.H. Chung, An experiment on the breakup of impinging droplets on a hot surface, Exp. Fluids 21 (1996) 118–123.
[18] J. Naber, P.V. Farrell, Hydrodynamics of droplet impingement on a heated surface, SAE Technical Paper 930919, 1993.
[19] S. Chandra, C.T. Avedisian, On the collision of a droplet with a solid surface, Proc. R. Soc. A – Math. Phys. Eng. Sci. 432 (1991) 13–41.
[20] A.B. Wang, C.H. Lin, C.C. Chen, The critical temperature of dry impact for tiny droplet impinging on a heated surface, Phys. Fluids 12 (2000) 1622–1625.
[21] J.D. Bernardin, C.J. Stebbins, I. Mudawar, Mapping of impact and heat transfer regimes of water drops impinging on a polished surface, Int. J. Heat Mass Transfer 40 (1997) 247–267.
[22] J.D. Bernardin, C.J. Stebbins, I. Mudawar, Effects of surface roughness on water droplet impact history and heat transfer regimes, Int. J. Heat Mass Transfer 40 (1997) 73–88.
[23] A.B. Wang, C.H. Lin, C.C. Cheng, Pattern analysis of a single droplet impinging onto a heated plate, Heat Transfer Asian Res. 34 (2005) 579–594.
[24] M. Khavari, C. Sun, D. Lohse, T. Tran, Fingering patterns during droplet impact on heated surfaces, Soft Matter 11 (2015) 3298–3303.
[25] T. Tran, H.J.J. Staat, A. Prosperetti, C. Sun, D. Lohse, Drop impact on superheated surfaces, Phys. Rev. Lett. 108 (2012) 036101.
[26] H.J. Staat, T. Tran, B. Geerdink, G. Riboux, C. Sun, J.M. Gordillo, D. Lohse, Phase diagram for droplet impact on superheated surfaces, J. Fluid Mech. 779 (2015) R3.
[27] G. Castanet, T. Lienart, F. Lemoine, Dynamics and temperature of droplets impacting onto a heated wall, Int. J. Heat Mass Transfer 52 (2009) 670–679.
[28] C. Mundo, M. Sommerfeld, C. Tropea, Droplet-wall collisions: experimental studies of the deformation and breakup process, Int. J. Multiphase Flow 21 (1995) 151–173.
[29] S.G. Kandlikar, M.E. Steinke, A. Singh, Effects of Weber number and surface temperature on the boiling and spreading characteristics of impinging water droplets, 35th National Heat Transfer Conference, in: 35th National Heat Transfer Conference, Anaheim, USA, 2001.
[30] M. Shirota, M.A. van Limbeek, C. Sun, A. Prosperetti, D. Lohse, Dynamic Leidenfrost effect: relevant time and length scales, Phys. Rev. Lett. 116 (2015) 064501.
[31] M.A. van Limbeek, M. Shirota, P. Sleutel, C. Sun, A. Prosperetti, D. Lohse, Vapour cooling of poorly conducting hot substrates increases the dynamic Leidenfrost temperature, Int. J. Heat Mass Transfer 97 (2016) 101–109.
[32] G. Liang, S. Shen, Y. Guo, J. Zhang, Boiling from liquid drops impact on a heated wall, Int. J. Heat Mass Transfer 100 (2016) 48–57.
[33] G. Liang, I. Mudawar, Review of mass and momentum interactions during drop impact on a liquid film, Int. J. Heat Mass Transfer 101 (2016) 577–599.
[34] M. di Marzo, D.D. Evans, Evaporation of a water droplet deposited on a hot high thermal conductivity surface, J. Heat Transfer 111 (1989) 210–213.
[35] M. Francois, W. Shyy, Computations of drop dynamics with the immersed boundary method, part 2: drop impact and heat transfer, Numer. Heat Transfer B 44 (2003) 119–143.
[36] M. di Marzo, P. Tartarini, Y. Liao, D.D. Evans, H. Baum, Evaporative cooling due to a gently deposited droplet, Int. J. Heat Mass Transfer 36 (1993) 4133–4139.
[37] O.E. Ruiz, W.Z. Black, Evaporation of water droplets placed on a heated horizontal surface, J. Heat Transfer 124 (2002) 854–863.
[38] E. Berberović, I.V. Roisman, S. Jakirlić, C. Tropea, Inertia dominated flow and heat transfer in liquid drop spreading on a hot substrate, Int. J. Heat Fluid Flow 32 (2011) 785–795.
[39] G. Strotos, M. Gavaises, A. Theodorakakos, G. Bergeles, Numerical investigation on the evaporation of droplets depositing on heated surfaces at low Weber numbers, Int. J. Heat Mass Transfer 51 (2008) 1516–1529.
[40] S. Zhang, G. Gogos, Film evaporation of a spherical droplet over a hot surface: fluid mechanics and heat/mass transfer analysis, J. Fluid Mech. 222 (1991) 543–563.
[41] S. Chandra, M. di Marzo, Y.M. Qiao, P. Tartarini, Effect of liquid-solid contact angle on droplet evaporation, Fire Saf. J. 27 (1996) 141–158.
[42] Y. Guo, S. Shen, S. Quan, Numerical simulation of dynamics of droplet impact on heated flat solid surface, Int. J. Low-Carbon Technol. 8 (2013) 134–139.
[43] G. Liang, X. Mu, Y. Guo, S. Shen, S. Quan, J. Zhang, Contact vaporization of an impacting drop on heated surfaces, Exp. Therm. Fluid Sci. 74 (2016) 73–80.
[44] J. Fukai, Y. Shiiba, O. Miyatake, Theoretical study of droplet impingement on a solid surface below the Leidenfrost temperature, Int. J. Heat Mass Transfer 40 (1997) 2490–2492.
[45] Q. Cui, S. Chandra, S. Mccahan, The effect of dissolving gases or solids in water droplets boiling on a hot surface, J. Heat Transfer 123 (2001) 719–728.
[46] V.E. Nakoryakov, S.Y. Misyura, S.L. Elistratov, The behavior of water droplets on the heated surface, Int. J. Heat Mass Transfer 55 (2012) 6609–6617.
[47] G. Strotos, M. Gavaises, A. Theodorakakos, G. Bergeles, Numerical investigation of the cooling effectiveness of a droplet impinging on a heated surface, Int. J. Heat Mass Transfer 51 (2008) 4728–4742.
[48] S. Herbert, S. Fischer, T. Gambaryan-Roisman, P. Stephan, Local heat transfer and phase change phenomena during single drop impingement on a hot surface, Int. J. Heat Mass Transfer 61 (2013) 605–614.
[49] S. Herbert, T. Gambaryan-Roisman, P. Stephan, Influence of the governing dimensionless parameters on heat transfer during single drop impingement onto a hot wall, Colloid Surfaces A 432 (2013) 57–63.
[50] W.M. Healy, J.G. Hartley, S.I. Abdel-Khalik, On the validity of the adiabatic spreading assumption in droplet impact cooling, Int. J. Heat Mass Transfer 44 (2001) 3869–3881.
[51] Y. Ge, L.S. Fan, 3-D modeling of the dynamics and heat transfer characteristics of subcooled droplet impact on a surface with film boiling, Int. J. Heat Mass Transfer 49 (2006) 4231–4249.
[52] W. Deng, A. Gomez, The role of electric charge in microdroplets impacting on conducting surfaces, Phys. Fluids 22 (2010) 051703.
[53] R. Srikar, T. Gambaryan-Roisman, C. Steffes, P. Stephan, C. Tropea, A. Yarin, Nanofiber coating of surfaces for intensification of drop or spray impact cooling, Int. J. Heat Mass Transfer 52 (2009) 5814–5826.
[54] C.M. Weickgenannt, Y. Zhang, A.N. Lembach, I.V. Roisman, T. Gambaryan-Roisman, A.L. Yarin, C. Tropea, Nonisothermal drop impact and evaporation on polymer nanofiber mats, Phys. Rev. E 83 (2011) 036305.
[55] S.L. Manzello, J.C. Yang, An experimental investigation of water droplet impingement on a heated wax surface, Int. J. Heat Mass Transfer 47 (2004) 1701–1709.
[56] S.L. Manzello, J.C. Yang, On the collision dynamics of a water droplet containing an additive on a heated solid surface, Proc. R. Soc. A – Math. Phys. Eng. Sci. 458 (2002) 2417–2444.
[57] A. Alizadeh, V. Bahadur, S. Zhong, W. Shang, R. Li, J. Ruud, M. Yamada, L. Ge, A. Dhinojwala, M. Sohal, Temperature dependent droplet impact dynamics on flat and textured surfaces, Appl. Phys. Lett. 100 (2012) 111601.
[58] J.H. Moon, M. Cho, S.H. Lee, Dynamic wetting and heat transfer characteristics of a liquid droplet impinging on heated textured surfaces, Int. J. Heat Mass Transfer 97 (2016) 308–317.
[59] M. Seki, H. Kawamura, K. Sanokawa, Transient temperature profile of a hot wall due to an impinging liquid droplet, J. Heat Transfer 100 (1978) 167–169.
[60] L. Tarozzi, A. Muscio, P. Tartarini, Experimental tests of dropwise cooling on infrared-transparent media, Exp. Therm. Fluid Sci. 31 (2007) 857–865.
[61] R. Bhardwaj, J.P. Longtin, D. Attinger, A numerical investigation on the influence of liquid properties and interfacial heat transfer during microdroplet deposition onto a glass substrate, Int. J. Heat Mass Transfer 50 (2007) 2912–2923.
[62] J.D. Bernardin, I. Mudawar, C.B. Walsh, E.I. Franses, Contact angle temperature dependence for water droplets on practical aluminum surfaces, Int. J. Heat Mass Transfer 40 (1997) 1017–1033.
[63] S.G. Kandlikar, M.E. Steinke, Contact angles and interface behavior during rapid evaporation of liquid on a heated surface, Int. J. Heat Mass Transfer 45 (2002) 3771–3780.
[64] S.G. Kandlikar, M.E. Steinke, Contact angles of droplets during spread and recoil after impinging on a heated surface, Chem. Eng. Res. Des. 79 (2001) 491–498.
[65] J.H. Moon, D.Y. Kim, S.H. Lee, Spreading and receding characteristics of a non-Newtonian droplet impinging on a heated surface, Exp. Therm. Fluid Sci. 57 (2014) 94–101.
[66] H. Hu, R.G. Larson, Evaporation of a sessile droplet on a substrate, J. Phys. Chem. B 106 (2002) 1334–1344.
[67] Y.M. Qiao, S. Chandra, Experiments on adding a surfactant to water drops boiling on a hot surface, Proc. R. Soc. A – Math. Phys. Eng. Sci. 453 (1997) 673–689.
[68] J. Rymkiewicz, Z. Zapalowicz, Analysis of the evaporation process for water droplet on flat heated surface, Int. Commun. Heat Mass Transfer 20 (1993) 687–697.
[69] E.F. Crafton, W.Z. Black, Heat transfer and evaporation rates of small liquid droplets on heated horizontal surfaces, Int. J. Heat Mass Transfer 47 (2004) 1187–1200.
[70] J. Shen, C. Graber, J. Liburdy, D. Pence, V. Narayanan, Simultaneous droplet impingement dynamics and heat transfer on nano-structured surfaces, Exp. Therm. Fluid Sci. 34 (2010) 496–503.

[71] T. Lim, S. Han, J. Chung, J.T. Chung, S. Ko, C.P. Grigoropoulos, Experimental study on spreading and evaporation of inkjet printed pico-liter droplet on a heated substrate, Int. J. Heat Mass Transfer 52 (2009) 431–441.
[72] C. Bonacina, S. Del Giudice, G. Comini, Dropwise evaporation, J. Heat Transfer 101 (1979) 441–446.
[73] C. Sodtke, V.S. Ajaev, P. Stephan, Evaporation of thin liquid droplets on heated surfaces, Heat Mass Transfer 43 (2007) 649–657.
[74] J. Lee, J. Kim, K.T. Kiger, Time- and space-resolved heat transfer characteristics of single droplet cooling using microscale heater arrays, Int. J. Heat Fluid Flow 22 (2001) 188–200.
[75] M. Guilizzoni, G. Sotgia, Experimental analysis on the shape and evaporation of water drops on high effusivity, microfinned surfaces, Exp. Therm. Fluid Sci. 34 (2010) 93–103.
[76] X. Li, X. Ma, Z. Lan, Behavioral patterns of drop impingement onto rigid substrates with a wide range of wettability and different surface temperatures, AIChE J. 55 (2009) 1983–1992.
[77] K. Sefiane, L. Tadrist, M. Douglas, Experimental study of evaporating water–ethanol mixture sessile drop: influence of concentration, Int. J. Heat Mass Transfer 46 (2003) 4527–4534.
[78] P. Tartarini, G. Lorenzini, M.R. Randi, Experimental study of water droplet boiling on hot, non-porous surfaces, Heat Mass Transfer 34 (1999) 437–447.
[79] T. Okawa, K. Nagano, T. Hirano, Boiling heat transfer during single nanofluid drop impacts onto a hot wall, Exp. Therm. Fluid Sci. 36 (2012) 78–85.
[80] T.Y. Xiong, M.C. Yuen, Evaporation of a liquid droplet on a hot plate, Int. J. Heat Mass Transfer 34 (1991) 1881–1894.
[81] A.S. Moita, A.L.N. Moreira, Boiling Morphology and Heat Removal of Impinging Coolant Droplets, ILASS, Como Lake, Italy, 2008.
[82] J.D. Bernardin, I. Mudawar, Film boiling heat transfer of droplet streams and sprays, Int. J. Heat Mass Transfer 40 (1997) 2579–2593.
[83] J.C. Chen, K.K. Hsu, Heat transfer during liquid contact on superheated surfaces, J. Heat Transfer 117 (1995) 693–697.
[84] J.Y. Park, A. Gardner, W.P. King, D.G. Cahill, Droplet impingement and vapor layer formation on hot hydrophobic surfaces, J. Heat Transfer 136 (2014) 092902.
[85] J.Y. Park, C.-K. Min, S. Granick, D.G. Cahill, Residence time and heat transfer when water droplets hit a scalding surface, J. Heat Transfer 134 (2012) 101503.
[86] S.G. Kandlikar, M.E. Steinke, High-speed photographic investigation of liquid-vapor interface and contact line movement during CHF and transition boiling, in: Proc. International Mechanical Engineering Congress and Exposition, New York, 2001, pp. 323–330.
[87] F. McGinnis, J. Holman, Individual droplet heat-transfer rates for splattering on hot surfaces, Int. J. Heat Mass Transfer 12 (1969) 95–108.
[88] J. Holman, P. Jenkins, F. Sullivan, Experiments on individual droplet heat transfer rates, Int. J. Heat Mass Transfer 15 (1972) 1489–1495.
[89] G. Duursma, K. Sefiane, A. Kennedy, Experimental studies of nanofluid droplets in spray cooling, Heat Transfer Eng. 30 (2009) 1108–1120.
[90] S. Akhtar, G.G. Nasr, A.J. Yule, Characteristics of water droplet impaction behavior on a polished steel heated surface: Part I, Atom. Sprays 17 (2007) 659–681.
[91] A.S. Moita, A.L.N. Moreira, I.V. Roisman, Heat transfer during drop impact onto a heated solid surface, in: Proc. 14th International Heat Transfer Conference, Washington DC, USA, 2010.
[92] N.Z. Mehdizadeh, S. Chandra, Boiling during high-velocity impact of water droplets on a hot stainless steel surface, Proc. R. Soc. A – Math. Physi. Eng. Sci. 462 (2006) 3115–3131.
[93] H. Fujimoto, Y. Oku, T. Ogihara, H. Takuda, Hydrodynamics and boiling phenomena of water droplets impinging on hot solid, Int. J. Multiphase Flow 36 (2010) 620–642.
[94] G.E. Cossali, M. Marengo, M. Santini, Secondary atomisation produced by single drop vertical impacts onto heated surfaces, Exp. Therm. Fluid Sci. 29 (2005) 937–946.
[95] G.E. Cossali, M. Marengo, M. Santini, Thermally induced secondary drop atomisation by single drop impact onto heated surfaces, Int. J. Heat Fluid Flow 29 (2008) 167–177.
[96] H. Chaves, A.M. Kubitzek, F. Obermeier, Dynamic processes occurring during the spreading of thin liquid films produced by drop impact on hot walls, Int. J. Heat Fluid Flow 20 (1999) 470–476.
[97] Y.M. Qiao, S. Chandra, Boiling of droplets on a hot surface in low gravity, Int. J. Heat Mass Transfer 39 (1996) 1379–1393.
[98] A.S. Moita, A.L.N. Moreira, Drop impacts onto cold and heated rigid surfaces: Morphological comparisons, disintegration limits and secondary atomization, Int. J. Heat Fluid Flow 28 (2007) 735–752.
[99] A.S. Moita, A.L.N. Moreira, Development of empirical correlations to predict the secondary droplet size of impacting droplets onto heated surfaces, Exp. Fluids 47 (2009) 755–768.
[100] S. Chandra, C. Avedisian, Observations of droplet impingement on a ceramic porous surface, Int. J. Heat Mass Transfer 35 (1992) 2377–2388.
[101] N. Nikolopoulos, A. Theodorakakos, G. Bergeles, A numerical investigation of the evaporation process of a liquid droplet impinging onto a hot substrate, Int. J. Heat Mass Transfer 50 (2007) 303–319.
[102] L. Qiu, S. Dubey, F.H. Choo, F. Duan, The transitions of time-independent spreading diameter and splashing angle when a droplet train impinging onto a hot surface, RSC Adv. 6 (2016) 13644–13652.
[103] J.G. Leidenfrost, On the fixation of water in diverse fire, Int. J. Heat Mass Transfer 9 (1966) 1153–1166.
[104] B.S. Gottfried, C.J. Lee, K.J. Bell, The leidenfrost phenomenon: film boiling of liquid droplets on a flat plate, Int. J. Heat Mass Transfer 9 (1966) 1167–1188.
[105] J. Burton, A. Sharpe, R. van der Veen, A. Franco, S. Nagel, Geometry of the vapor layer under a Leidenfrost drop, Phys. Rev. Lett. 109 (2012) 074301.
[106] K. Anders, N. Roth, A. Frohn, The velocity change of ethanol droplets during collision with a wall analysed by image processing, Exp. Fluids 15 (1993) 91–96.
[107] G.F. Hewitt, G.L. Shires, Y.V. Polezhaev, International Encyclopedia of Heat & Mass Transfer, CRC Press, New York, 1997.
[108] D. Quéré, Leidenfrost dynamics, Ann. Rev. Fluid Mech. 45 (2013) 197–215.
[109] D. Brutin, Droplet Wetting and Evaporation: from Pure to Complex Fluids, Academic Press, 2015, pp. 85–99.
[110] J. Bernardin, I. Mudawar, The Leidenfrost point: experimental study and assessment of existing models, J. Heat Transfer 121 (1999) 894–903.
[111] J.D. Bernardin, I. Mudawar, A cavity activation and bubble growth model of the Leidenfrost point, J. Heat Transfer 124 (2002) 864–874.
[112] P. Testa, L. Nicotra, Influence of pressure on the Leidenfrost temperature and on extracted heat fluxes in the transient mode and low pressure, J. Heat Transfer 108 (1986) 916–921.
[113] F. Celestini, T. Frisch, Y. Pomeau, Room temperature water Leidenfrost droplets, Soft Matter 9 (2013) 9535–9538.
[114] G.S. Emmerson, The effect of pressure and surface material on the Leidenfrost point of discrete drops of water, Int. J. Heat Mass Transfer 18 (1975) 381–386.
[115] G. Emmerson, C. Snoek, The effect of pressure on the Leidenfrost point of discrete drops of water and freon on a brass surface, Int. J. Heat Mass Transfer 21 (1978) 1081–1086.
[116] C. Avedisian, J. Koplik, Leidenfrost boiling of methanol droplets on hot porous/ceramic surfaces, Int. J. Heat Mass Transfer 30 (1987) 379–393.
[117] H. Kim, B. Truong, J. Buongiorno, L.-W. Hu, On the effect of surface roughness height, wettability, and nanoporosity on Leidenfrost phenomena, Appl. Phys. Lett. 98 (2011) 083121.
[118] H. Kim, B. Truong, J. Buongiorno, L.-W. Hu, Effects of micro/nano-scale surface characteristics on the Leidenfrost point temperature of water, J. Therm. Sci. Tech. 7 (2012) 453–462.
[119] H.-M. Kwon, J.C. Bird, K.K. Varanasi, Increasing Leidenfrost point using micro-nano hierarchical surface structures, Appl. Phys. Lett. 103 (2013) 201601.
[120] C. Kruse, T. Anderson, C. Wilson, C. Zuhlke, D. Alexander, G. Gogos, S. Ndao, Extraordinary shifts of the Leidenfrost temperature from multiscale micro/nanostructured surfaces, Langmuir 29 (2013) 9798–9806.
[121] R.A. Munoz, D. Beving, Y. Yan, Hydrophilic zeolite coatings for improved heat transfer, Ind. Eng. Chem. Res. 44 (2005) 4310–4315.
[122] D. Arnaldo del Cerro, A.I.G. Marín, G.R. Römer, B. Pathiraj, D. Lohse, A.J. Huis in't Veld, Leidenfrost point reduction on micropatterned metallic surfaces, Langmuir 28 (2012) 15106–15110.
[123] Y. Takata, S. Hidaka, A. Yamashita, H. Yamamoto, Evaporation of water drop on a plasma-irradiated hydrophilic surface, Int. J. Heat Fluid Flow 25 (2004) 320–328.
[124] Y. Takata, S. Hidaka, J. Cao, T. Nakamura, H. Yamamoto, M. Masuda, T. Ito, Effect of surface wettability on boiling and evaporation, Energy 30 (2005) 209–220.
[125] C.-K. Huang, V.P. Carey, The effects of dissolved salt on the Leidenfrost transition, Int. J. Heat Mass Transfer 50 (2007) 269–282.
[126] L. Maquet, M. Brandenbourger, B. Sobac, A. Biance, P. Colinet, S. Dorbolo, Leidenfrost drops: Effect of gravity, Europhys. Lett. 110 (2015) 24001.
[127] F. Celestini, G. Kirstetter, Effect of an electric field on a Leidenfrost droplet, Soft Matter 8 (2012) 5992–5995.
[128] H. Linke, B. Alemán, L. Melling, M. Taormina, M. Francis, C. Dow-Hygelund, V. Narayanan, R. Taylor, A. Stout, Self-propelled Leidenfrost droplets, Phys. Rev. Lett. 96 (2006) 154502.
[129] D. Quéré, A. Ajdari, Liquid drops: Surfing the hot spot, Nat. Mater. 5 (2006) 429–430.
[130] G. Lagubeau, M. Le Merrer, C. Clanet, D. Quéré, Leidenfrost on a ratchet, Nat. Phys. 7 (2011) 395–398.
[131] G. Dupeux, M. Le Merrer, G. Lagubeau, C. Clanet, S. Hardt, D. Quéré, Viscous mechanism for Leidenfrost propulsion on a ratchet, Europhys. Lett. 96 (2011) 58001.
[132] T. Baier, G. Dupeux, S. Herbert, S. Hardt, D. Quéré, Propulsion mechanisms for Leidenfrost solids on ratchets, Phys. Rev. E 87 (2013) 021001.
[133] G. Dupeux, P. Bourrianne, Q. Magdelaine, C. Clanet, D. Quéré, Propulsion on a superhydrophobic ratchet, Sci. Rep. 4 (2014) 5280.
[134] A.G. Marin, D.A. del Cerro, G.R. Römer, B. Pathiraj, D. Lohse, Capillary droplets on Leidenfrost micro-ratchets, Phys. Fluids 24 (2012) 122001.
[135] J.T. Ok, E. Lopez-Ona, D.E. Nikitopoulos, H. Wong, S. Park, Propulsion of droplets on micro-and sub-micron ratchet surfaces in the Leidenfrost temperature regime, Microfluid. Nanofluid. 10 (2011) 1045–1054.
[136] T.R. Cousins, R.E. Goldstein, J.W. Jaworski, A.I. Pesci, A ratchet trap for Leidenfrost drops, J. Fluid Mech. 696 (2012) 215–227.
[137] Q. Li, Q. Kang, M. Francois, A. Hu, Lattice Boltzmann modeling of self-propelled Leidenfrost droplets on ratchet surfaces, Soft Matter 12 (2016) 302–312.
[138] N. Nagai, S. Nishio, Leidenfrost temperature on an extremely smooth surface, Exp. Therm. Fluid Sci. 12 (1996) 373–379.
[139] K. Baumeister, F. Simon, Leidenfrost temperature—its correlation for liquid metals, cryogens, hydrocarbons, and water, J. Heat Transfer 95 (1973) 166–173.

[140] B. Richter, K. Dullenkopf, H.J. Bauer, Investigation of secondary droplet characteristics produced by an isooctane drop chain impact onto a heated piston surface, Exp. Fluids 39 (2005) 351–363.
[141] M. Rein, Drop-surface interactions, Springer, Vienna, 2002, pp. 185–217.
[142] C. Pedersen, An experimental study of the dynamic behavior and heat transfer characteristics of water droplets impinging upon a heated surface, Int. J. Heat Mass Transfer 13 (1970) 369–381.
[143] G.P. Celata, M. Cumo, A. Mariani, G. Zummo, Visualization of the impact of water drops on a hot surface: effect of drop velocity and surface inclination, Heat Mass Transfer 42 (2006) 885–890.
[144] S.C. Yao, K.Y. Cai, The dynamics and leidenfrost temperature of drops impacting on a hot surface at small angles, Exp. Therm. Fluid Sci. 1 (1988) 363–371.
[145] V. Bertola, K. Sefiane, Controlling secondary atomization during drop impact on hot surfaces by polymer additives, Phys. Fluids 17 (2005) 108104.
[146] V. Bertola, Drop impact on a hot surface: effect of a polymer additive, Experiments Fluids 37 (2004) 653–664.
[147] B. Nigmatulin, N. Vasiliev, V. Guguchkin, Interaction between liquid droplets and heated surface, Wärme-und Stoffübertragung 28 (1993) 313–319.
[148] A. Karl, A. Frohn, Experimental investigation of interaction processes between droplets and hot walls, Phys. Fluids 12 (2000) 785–796.
[149] T. Tran, H.J.J. Staat, A. Susarrey-Arce, T.C. Foertsch, A. Van Houselt, H.J.G.E. Gardeniers, A. Prosperetti, D. Lohse, C. Sun, Droplet impact on superheated micro-structured surfaces, Soft Matter 9 (2013) 3272–3282.
[150] J. Senda, K. Yamada, H. Fujimoto, H. Miki, The heat transfer characteristics of a small droplet impinging upon a hot surface, JSME Int J. B 31 (1988) 105–111.
[151] C.M. Weickgenannt, Y. Zhang, S. Sinha-Ray, I.V. Roisman, T. Gambaryan-Roisman, C. Tropea, A.L. Yarin, Inverse-Leidenfrost phenomenon on nanofiber mats on hot surfaces, Phys. Rev. E 84 (2011) 036310.
[152] H. Nair, H.J. Staat, T. Tran, A. van Houselt, A. Prosperetti, D. Lohse, C. Sun, The Leidenfrost temperature increase for impacting droplets on carbon-nanofiber surfaces, Soft Matter 10 (2014) 2102–2109.
[153] B.T. Ng, Y.M. Hung, M.K. Tan, Suppression of the Leidenfrost effect via low frequency vibrations, Soft Matter 11 (2015) 775–784.
[154] J.D. Bernardin, I. Mudawar, A Leidenfrost point model for impinging droplets and sprays, J. Heat Transfer 126 (2004) 272–278.
[155] O.G. Engel, Note on particle velocity in collisions between liquid drops and solids, J. Res. Nat. Bureau Stand. A 64 (1960) 497–498.
[156] O.G. Engel, Waterdrop collisions with solid surfaces, J. Res. Nat. Bureau Stand. A 54 (1955) 281–298.
[157] A.L. Biance, C. Clanet, D. Quéré, Leidenfrost drops, Phys. Fluids 15 (2003) 1632–1637.
[158] M. Prat, P. Schmitz, D. Poulikakos, On the effect of surface roughness on the vapor flow under Leidenfrost-levitated droplets, J. Fluid. Eng. 117 (1995) 519–525.
[159] F. Celestini, T. Frisch, Y. Pomeau, Take off of small Leidenfrost droplets, Phys. Rev. Lett. 109 (2012) 034501.
[160] Y. Ge, L.S. Fan, Three-dimensional simulation of impingement of a liquid droplet on a flat surface in the Leidenfrost regime, Phys. Fluids 17 (2005) 027104.
[161] D. Chatzikyriakou, S.P. Walker, G.F. Hewitt, C. Narayanan, D. Lakehal, Comparison of measured and modelled droplet–hot wall interactions, Appl. Therm.Eng. 29 (2009) 1398–1405.
[162] L.H.J. Wachters, H. Bonne, H.J. Van Nouhuis, The heat transfer from a hot horizontal plate to sessile water drops in the spheroidal state, Chem. Eng. Sci. 21 (1966) 923–936.
[163] S. Inada, Y. Miyasaka, K. Sakamoto, K. Hojo, Liquid-solid contact state and fluctuation of the vapor film thickness of a drop impinging on a heated surface, J. Chem. Eng. Jpn. 21 (1988) 463–468.
[164] S. Thoroddsen, T. Etoh, K. Takehara, N. Ootsuka, Y. Hatsuki, The air bubble entrapped under a drop impacting on a solid surface, J. Fluid Mech. 545 (2005) 203–212.
[165] S. Akhtar, G.G. Nasr, Characteristics of water droplet impaction behavior on a polished steel heated surface: Part II, Atomization. Sprays 17 (2007) 683–729.
[166] N. Hatta, H. Fujimoto, K. Kinoshita, H. Takuda, Experimental study of deformation mechanism of a water droplet impinging on hot metallic surfaces above the Leidenfrost temperature: (Data bank contribution), J. Fluids Eng. 119 (1997) 692–699.
[167] T. Ueda, T. Enomoto, M. Kanetsuki, Heat transfer characteristics and dynamic behavior of saturated droplets impinging on a heated vertical surface, Bull. JSME 22 (1979) 724–732.
[168] S.-L. Chiu, T.-H. Lin, Experiment on the dynamics of a compound drop impinging on a hot surface, Physics Fluids 17 (2005) 122103.
[169] A.L. Biance, C. Pirat, C. Ybert, Drop fragmentation due to hole formation during Leidenfrost impact, Phys. Fluids 23 (2011) 022104.
[170] D. Chatzikyriakou, S.P. Walker, G.F. Hewitt, The contribution of non-wetting droplets to direct cooling of the fuel during PWR post-LOCA reflood, Nucl. Eng. Des. 240 (2010) 3108–3114.
[171] D. Chatzikyriakou, S. Walker, B. Belhouachi, C. Narayanan, D. Lakehal, G. Hewitt, Three dimensional modeling of the hydrodynamics of oblique droplet-hot wall interactions during the reflood phase after a LOCA, J. Eng. Gas Turbines Power 132 (2010) 102914.
[172] B.S. Kang, D.H. Lee, On the dynamic behavior of a liquid droplet impacting upon an inclined heated surface, Exp. Fluids 29 (2000) 380–387.
[173] R.H. Chen, S.L. Chiu, T.H. Lin, On the collision behaviors of a diesel drop impinging on a hot surface, Exp. Therm. Fluid Sci. 32 (2007) 587–595.
[174] R. Kannan, D. Sivakumar, Drop impact process on a hydrophobic grooved surface, Colloids Surf. A 317 (2008) 694–704.
[175] R. Rioboo, M. Voué, A. Vaillant, J. De Coninck, Drop impact on porous superhydrophobic polymer surfaces, Langmuir 24 (2008) 14074–14077.
[176] G. Liang, Y. Yang, Y. Guo, N. Zhen, S. Shen, Rebound and spreading during a drop impact on wetted cylinders, Exp. Therm. Fluid Sci. 52 (2014) 97–103.
[177] G. Liang, Y. Guo, Y. Yang, S. Guo, S. Shen, Special phenomena from a single liquid drop impact on wetted cylindrical surfaces, Exp. Therm. Fluid Sci. 51 (2013) 18–27.
[178] B. Ricther, K. Dullenkopf, S. Wittig, Wall impact of single droplets under conditions of DISI-Engines, in: Proc. 9th International Conference of Liquid Atomization and Spray Systems, Sorrento, Italy, 2003.
[179] C. Antonini, I. Bernagozzi, S. Jung, D. Poulikakos, M. Marengo, Water drops dancing on ice: how sublimation leads to drop rebound, Physical Rev. Lett. 111 (2013) 014501.
[180] A.L. Biance, F. Chevy, C. Clanet, G. Lagubeau, D. Quéré, On the elasticity of an inertial liquid shock, J. Fluid Mech. 554 (2006) 47–66.
[181] A. Karl, K. Anders, M. Rieber, A. Frohn, Deformation of liquid droplets during collisions with hot walls: experimental and numerical results, Part. Part. Syst. Charact. 13 (1996) 186–191.
[182] S. Mitra, M.J. Sathe, E. Doroodchi, R. Utikar, M.K. Shah, V. Pareek, J.B. Joshi, G. M. Evans, Droplet impact dynamics on a spherical particle, Chem. Eng. Sci. 100 (2013) 105–119.
[183] D.J.E. Harvie, D.F. Fletcher, A hydrodynamic and thermodynamic simulation of droplet impacts on hot surfaces, Part II: validation and applications, Int. J. Heat Mass Transfer 44 (2001) 2643–2659.
[184] D.J.E. Harvie, D.F. Fletcher, A hydrodynamic and thermodynamic simulation of droplet impacts on hot surfaces, Part I: theoretical model, Int. J. Heat Mass Transfer 44 (2001) 2633–2642.
[185] Z. Yu, Y. Ge, L.S. Fan, Multi-scale simulation of oblique collisions of a droplet on a surface in the Leidenfrost regime, Chem. Eng. Sci. 62 (2007) 3462–3472.
[186] Y. Ge, L.S. Fan, Droplet–particle collision mechanics with film-boiling evaporation, J. Fluid Mech. 573 (2007) 311–337.
[187] H. Fujimoto, N. Hatta, Deformation and rebounding processes of a water droplet impinging on a flat surface above Leidenfrost temperature, J. Fluids Eng. 118 (1996) 142–149.
[188] A.V. Chizhov, K. Takayama, The impact of compressible liquid droplet on hot rigid surface, Int. J. Heat Mass Transfer 47 (2004) 1391–1401.
[189] K. Makino, I. Michiyoshi, The behavior of a water droplet on heated surfaces, Int. J. Heat Mass Transfer 27 (1984) 781–791.
[190] L. Rayleigh, On the capillary phenomena of jets, Proc. R. Soc. London 29 (1879) 71–97.
[191] D. Richard, C. Clanet, D. Quéré, Surface phenomena: contact time of a bouncing drop, Nature 417 (2002), 811-811.
[192] F. Akao, K. Araki, S. Mori, A. Moriyama, Deformation behaviours of a liquid droplet Impinging onto hot metal surface, Trans. Iron Steel Inst. Jpn. 20 (1980) 737–743.
[193] R.H. Chen, S.L. Chiu, T.H. Lin, Resident time of a compound drop impinging on a hot surface, Appl. Therm. Eng. 27 (2007) 2079–2085.
[194] E.R. Negeed, M. Albeirutty, S.F. AL-Sharif, S. Hidaka, Y. Takata, Dynamic behavior of a small water droplet impact onto a heated hydrophilic surface, J. Heat Transfer 138 (2016) 042901.
[195] S. Shen, F. Bi, Y. Guo, Simulation of droplets impact on curved surfaces with lattice Boltzmann method, Int. J. Heat Mass Transfer 55 (2012) 6938–6943.
[196] Z. Zhao, D. Poulikakos, J. Fukai, Heat transfer and fluid dynamics during the collision of a liquid droplet on a substrate—I. Modeling, Int. J. Heat Mass Transfer 39 (1996) 2771–2789.
[197] S.L. Manzello, J.C. Yang, An experimental study of high Weber number impact of methoxy-nonafluorobutane C4F9OCH3 (HFE-7100) and n-heptane droplets on a heated solid surface, Int. J. Heat Mass Transfer 45 (2002) 3961–3971.
[198] V. Bertola, An experimental study of bouncing Leidenfrost drops: comparison between Newtonian and viscoelastic liquids, Int. J. Heat Mass Transfer 52 (2009) 1786–1793.
[199] E.R. Negeed, S. Hidaka, M. Kohno, Y. Takata, High speed camera investigation of the impingement of single water droplets on oxidized high temperature surfaces, Int. J. Therm. Sci. 63 (2013) 1–14.
[200] E.R. Negeed, N. Ishihara, K. Tagashira, S. Hidaka, M. Kohno, Y. Takata, Experimental study on the effect of surface conditions on evaporation of sprayed liquid droplet, Int. J. Therm. Sci. 49 (2010) 2250–2271.
[201] E.R. Negeed, S. Hidaka, M. Kohno, Y. Takata, Effect of the surface roughness and oxidation layer on the dynamic behavior of micrometric single water droplets impacting onto heated surfaces, Int. J. Therm. Sci. 70 (2013) 65–82.
[202] E.R. Negeed, M. Albeirutty, Y. Takata, Dynamic behavior of micrometric single water droplets impacting onto heated surfaces with TiO 2 hydrophilic coating, Int. J. Therm. Sci. 79 (2014) 1–17.
[203] G. Castanet, O. Caballina, F. Lemoine, Drop spreading at the impact in the Leidenfrost boiling, Phys. Fluids 27 (2015) 063302.
[204] C. Clanet, C. Béguin, D. Richard, D. Quéré, Maximal deformation of an impacting drop, J. Fluid Mech. 517 (2004) 199–208.
[205] P. Tsai, M.H. Hendrix, R.R. Dijkstra, L. Shui, D. Lohse, Microscopic structure influencing macroscopic splash at high Weber number, Soft Matter 7 (2011) 11325–11333.
[206] N. Hatta, H. Fujimoto, H. Takuda, K. Kinoshita, O. Takahashi, Collision dynamics of a water droplet impinging on a rigid surface above the Leidenfrost temperature, Steel Ins. Jpn. (ISIJ) Int. 35 (1995) 50–55.

[207] S. Akhtar, A. Yule, Droplet Impaction on a Heated Surface at High Weber Numbers, ILASS-Europe, Zurich, Switzerland, 2001.
[208] H. Lastakowski, F. Boyer, A.-L. Biance, C. Pirat, C. Ybert, Bridging local to global dynamics of drop impact onto solid substrates, J. Fluid Mech. 747 (2014) 103–118.
[209] B.S. Gottfried, K.J. Bell, Film boiling of spheroidal droplets. Leidenfrost phenomenon, Ind. Eng. Chem. Fundam. 5 (1966) 561–568.
[210] S. Inada, W.J. Yang, Film boiling heat transfer for saturated drops impinging on a heating surface, Int. J. Heat Mass Transfer 37 (1994) 2588–2591.
[211] N.M. Wruck, U. Renz, Transient Phase-change of Droplets Impacting on a Hot Wall, Wiley-VCH, Weinheim, 2007.
[212] M. Shi, T. Bai, J. Yu, Dynamic behavior and heat transfer of a liquid droplet impinging on a solid surface, Exp. Therm. Fluid Sci. 6 (1993) 202–207.
[213] H. Xie, Z. Zhou, A model for droplet evaporation near Leidenfrost point, Int. J. Heat Mass Transfer 50 (2007) 5328–5333.
[214] D. Chatzikyriakou, S.P. Walker, C.P. Hale, G.F. Hewitt, The measurement of heat transfer from hot surfaces to non-wetting droplets, Int. J. Heat Mass Transfer 54 (2011) 1432–1440.
[215] P. Dunand, G. Castanet, F. Lemoine, A two-color planar LIF technique to map the temperature of droplets impinging onto a heated wall, Exp. Fluids 52 (2012) 843–856.
[216] P. Dunand, G. Castanet, M. Gradeck, D. Maillet, F. Lemoine, Energy balance of droplets impinging onto a wall heated above the Leidenfrost temperature, Int. J. Heat Fluid Flow 44 (2013) 170–180.
[217] P. Dunand, G. Castanet, M. Gradeck, F. Lemoine, D. Maillet, Heat transfer of droplets impinging onto a wall above the Leidenfrost temperature, C. R. Méc. 341 (2013) 75–87.
[218] F.P. Buckingham, A. Haji-Sheikh, Cooling of high-temperature cylindrical surfaces using a water–air spray, J. Heat Transfer 117 (1995) 1018–1027.
[219] R. Thomas, M. Ganesa-Pillai, P.B. Aswath, K.L. Lawrence, A. Hajisheikh, Analytical/finite-element modeling and experimental verification of spray-cooling process in steel, Metall. Mater. Trans. A 29 (1998) 1485–1498.
[220] P. Pournaderi, A. Pishevar, A numerical investigation of droplet impact on a heated wall in the film boiling regime, Heat Mass Transfer 48 (2012) 1525–1538.
[221] V. Labeish, Thermohydrodynamic study of a drop impact against a heated surface, Exp. Therm. Fluid Sci. 8 (1994) 181–194.
[222] M. Gradeck, N. Seiler, P. Ruyer, D. Maillet, Heat transfer for Leidenfrost drops bouncing onto a hot surface, Exp. Therm. Fluid Sci. 47 (2013) 14–25.
[223] V. Labeish, A. Pimenov, Experimental study of heat transfer between a hot wall and impinging drops, J. Eng. Phys. Thermophys. 47 (1984) 1400–1406.
[224] K. Choi, J. Hong, Heat transfer characteristics of water droplets interacting with a rotating hot surface, Int. Commun. Heat Mass Transfer 17 (1990) 419–429.
[225] S. Chandra, S.D. Aziz, Leidenfrost evaporation of liquid nitrogen droplets, J. Heat Transfer 116 (1994) 999–1006.
[226] M. Fatehi, M. Kaviany, Analysis of levitation of saturated liquid droplets on permeable surfaces, Int. J. Heat Mass Transfer 33 (1990) 983–994.
[227] A.L.N. Moreira, A.S. Moita, E. Cossali, M. Marengo, M. Santini, Secondary atomization of water and isooctane drops impinging on tilted heated surfaces, Exp. Fluids 43 (2007) 297–313.
[228] G.E. Cossali, M. Marengo, M. Santini, Multiple drop impact on heated surface, in: Proceedings of the 9th ICLASS, Sorrento, Italy, 2003.
[229] G.E. Cossali, M. Marengo, M. Santini, Drop array impacts on heated surfaces: secondary atomization characteristics, in: 19th Annual Meeting of ILASS, Nottingham, UK, 2004.
[230] T. Minamikawa, H. Fujimoto, T. Hama, H. Takuda, Numerical simulation of two droplets impinging successively on a hot solid in the film boiling regime, Iron Steel Inst. Jpn. (ISIJ) Int. 48 (2008) 611–615.
[231] H. Fujimoto, A.Y. Tong, H. Takuda, Interaction phenomena of two water droplets successively impacting onto a solid surface, Int. J. Therm. Sci. 47 (2008) 229–236.
[232] B. Richter, K. Dullenkopf, H.J. Bauer, Investigation of secondary droplet characteristics produced during wall impact, in: Proc. 12th International Symposium Laser Techniques Application Fluid Mechanics, Lisbon, Portugal, 2004.